

EXPONENTIALLY CONVERGENT MULTISCALE METHODS FOR HIGH FREQUENCY HETEROGENEOUS HELMHOLTZ EQUATIONS*

YIFAN CHEN[†], THOMAS Y. HOU[†], AND YIXUAN WANG[†]

Abstract. In this paper, we present a multiscale framework for solving the Helmholtz equation in heterogeneous media without scale separation and in the high frequency regime where the wavenumber k can be large. The main innovation is that our methods achieve a nearly exponential rate of convergence with respect to the computational degrees of freedom, using a coarse grid of mesh size $O(1/k)$ without suffering from the well-known pollution effect. The key idea is a coarse-fine scale decomposition of the solution space that adapts to the media property and wavenumber; this decomposition is inspired by the multiscale finite element method. We show that the coarse part is of *low complexity* in the sense that it can be approximated with a nearly exponential rate of convergence via local basis functions, while the fine part is *local* such that it can be computed efficiently using the local information of the right hand side. The combination of the two parts yields the overall nearly exponential rate of convergence. We demonstrate the effectiveness of our methods theoretically and numerically; an exponential rate of convergence is consistently observed and confirmed. In addition, we observe the robustness of our methods regarding the high contrast in the media numerically.

Key words. The Helmholtz equation, Heterogeneous Media, High Frequency, Exponential Convergence, Multiscale Methods, High Contrast.

AMS subject classifications. 65N12, 65N15, 65N30, 31A35.

1. Introduction. This paper focuses on solving the Helmholtz equation in heterogeneous media and high frequency regimes. We consider the model problem in a bounded domain $\Omega \subset \mathbb{R}^d$ with a Lipschitz boundary Γ . For generality, the boundary can contain three disjoint parts $\Gamma = \Gamma_D \cup \Gamma_N \cup \Gamma_R$ where Γ_D, Γ_N and Γ_R correspond to the Dirichlet, Neumann and Robin type conditions, respectively. Given positive constants $A_{\min}, A_{\max}, \beta_{\min}, \beta_{\max}, V_{\min}, V_{\max}$ and functions $A, \beta, V : \Omega \rightarrow \mathbb{R}$ that satisfy $A_{\min} \leq A(x) \leq A_{\max}, \beta_{\min} \leq \beta(x) \leq \beta_{\max}$ and $V_{\min} \leq V(x) \leq V_{\max}$, the Helmholtz equation with homogeneous boundary conditions¹ is formulated as follows:

$$(1.1) \quad \begin{cases} -\nabla \cdot (A \nabla u) - k^2 V^2 u = f, & \text{in } \Omega \\ u = 0, & \text{on } \Gamma_D \\ A \nabla u \cdot \nu = T_k u, & \text{on } \Gamma_N \cup \Gamma_R. \end{cases}$$

Here, ν is the outer normal to the boundary. The boundary operator satisfies $T_k u = 0$ for $x \in \Gamma_N$ and $T_k u = ik\beta u$ for $x \in \Gamma_R$, where i denotes the imaginary number. The wavenumber k is real and positive, and functions u and f are complex-valued. The purpose of this paper is to design a multiscale method for solving (1.1) that achieves a nearly exponential rate of convergence with respect to the computational degrees of freedom.

1.1. Literature Review. The Helmholtz equation has been widely used in studying wave propagation in complex media. Numerical simulation of this equation still remains a challenging task, especially in the regime where the wavenumber

*Submitted to the editors DATE: TBA.

Funding: This research is in part supported by NSF Grants DMS-1912654 and DMS-1907977. Y. Chen is also grateful to the support from the Caltech Kortchak Scholar Program.

[†]Applied and Computational Mathematics, Caltech (yifanc@caltech.edu, hou@cms.caltech.edu, roywang@caltech.edu).

¹For simplicity of presentation, homogeneous boundary conditions are considered here. Generalization to non-homogeneous data is straightforward; see Section 5.3.

k is large. The main numerical difficulty lies in the highly oscillatory pattern of the solution. Furthermore, the operator in the equation is indefinite, which leads to severe instability issues for standard numerical solvers such as the finite element method (FEM). Indeed, a well-known pre-asymptotic effect called the pollution effect [3] can occur — that is, in order to get a reasonably accurate solution, the mesh size H in the FEM needs to be much smaller than $1/k$. This constraint on H is much stronger than the typical condition in the approximation theory for representing an oscillatory function with frequency k , where $H = O(1/k)$, i.e., a fixed number of grid points per wavelength, would suffice for an accurate approximate solution.

In the literature, there have been many attempts to overcome or alleviate the difficulty associated with the pollution effect. We highlight two methods, namely the hp -FEM and multiscale approaches, that can theoretically deal with the pollution effect under their model assumptions. The hp -FEM is proposed in [26, 27], which is a finite element method using local high order polynomials. It is shown that by choosing the degrees of local polynomials $p = O(\log k)$, the pollution effect can be suppressed in principle for the Helmholtz equation with constant A, V and β . Nevertheless, to the best of our knowledge, there have been no theoretical results for this methodology when these coefficients become rough. It is well-known that polynomials might behave arbitrarily bad even for elliptic equations with rough coefficients [2].

Multiscale methods, on the other hand, have long been developed to address the difficulty associated with rough coefficients in elliptic equations. In particular, we mention the LOD and Gamblets related approaches [25, 21, 33, 31, 32, 6] and variants of the multiscale finite element method (MsFEM) [23, 9, 22, 8, 13, 7] that are most related to this paper. Recently, the LOD method has been generalized into the case of Helmholtz equations with high wavenumber and heterogeneous media [34, 16, 5, 35]. They show that with a coarse mesh of size $O(H)$ and localized multiscale basis functions of support size $O(H \log(1/H) \log k)$, the pollution effect can be overcome once the stability constant of the solution operator of the Helmholtz equation is of at most polynomial growth. An error of at most $O(H)$ is established. Alternatively, from the perspective of MsFEM methodology, the authors in [15] introduce WMsFEM to address the pollution effect successfully. However, on the theoretical side, the number of basis functions in each element might be huge ($O(k)$) in order to achieve a reasonable accuracy. In contrast, our method in this paper, which can be viewed as a generalization of MsFEM, only requires $O(\log^{d+1} k)$ number of basis function in each element to handle the pollution effect. More importantly, our method yields an overall exponential rate of convergence thanks to a systematic decomposition and treatment of coarse and fine scale parts of the solution.

In addition to those methods mentioned above, there have also been several algorithms based on the MsFEM methodology [29, 14] or the HMM methodology [30] with particular empirical success for solving the Helmholtz equation. It is also worth noting that, in conjunction with designing a good discretization scheme as above, one could also consider fast solvers for the discrete linear system. See, for example, the method of sweeping preconditioners [10, 11, 36], where a preconditioning matrix is constructed to compute approximations of the Schur complements successively. Very recently, the LOD approach has also been combined with the hierarchical approach of Gamblets [20] to get a multiresolution solver for the discrete system.

1.2. Main Contributions. In this paper, we propose a multiscale framework for solving the Helmholtz equation in rough media and high frequency regimes, especially in dimension $d = 2$. Generalization to higher dimensions will be elaborated at

the end of this paper. The idea is based on a multiscale method in our previous work [7] for solving elliptic equations with rough coefficients in an exponentially convergent manner. This paper aims to extend this framework to the more challenging Helmholtz equation where the operator is non-Hermitian and indefinite. It is perhaps surprising that the techniques in multiscale methods for elliptic equations can be systematically adapted to the Helmholtz equation. We outline the main contributions of this paper below.

1. In studying the solution behavior of the Helmholtz equation (1.1), we introduce a coarse-fine scale decomposition of its solution space. This decomposition is adapted to the coarse mesh structure; a mesh size of $O(1/k)$ suffices to make this coarse-fine scale decomposition well defined. Moreover, the decomposition is adapted to the coefficients A, V, β and the wavenumber k .
2. Analytically, we show the fine scale part is of $O(H)$ in the energy norm, and it can be computed efficiently by solving the Helmholtz equations locally. Meanwhile, we prove that the space of the coarse scale part is of low complexity, such that there exist local multiscale basis functions that can approximate this part in a nearly exponentially convergent manner. These serve as the cornerstone of our multiscale numerical method.
3. Numerically, we propose a multiscale framework that solves the two parts separately. The nearly exponential rate of convergence in the energy norm and L^2 norm is theoretically proved in this paper.
4. Experimentally, we conduct extensive numerical tests and observe consistently that our multiscale methods give a nearly exponential rate of convergence, even for problems with high-contrast media. Based on these numerical studies, several recommendations for efficient implementations of our methods are provided, especially on how to design the offline and online computation to handle multiple right hand sides efficiently.

To the best of our knowledge, this multiscale framework is the first one that can be proved rigorously to achieve a nearly exponential rate of convergence in solving (1.1) with rough A, β, V and large k . We also remark that in principle, our multiscale algorithm can be applied to general Helmholtz equations numerically, while most of our theoretical results rely on analytical properties of the solution to equation (1.1), related to the well-posedness, stability and C^α estimates. Therefore, typical conditions (usually very mild) of these analytical properties will be assumed in this paper, in order to get a rigorous theory. We will mention several references to these results in this paper. Some numerical examples in which these assumptions are violated will be also presented to illustrate the effectiveness of our algorithm in a general context.

1.3. Organization. The rest of this paper is organized as follows. In Section 2, we review preliminary results for the Helmholtz equation, including the well-posedness, stability, adjoint problems, and C^α estimates. Section 3 is devoted to analyzing the solution space based on a coarse-fine scale decomposition. Moreover, the computational properties of the coarse and fine parts are rigorously studied in detail. Building upon these properties, in Section 4 we develop the multiscale computational framework and prove the nearly exponential rate of convergence for our multiscale methods. The detailed numerical algorithms are discussed and implemented in Section 5 for several Helmholtz equations. To improve the readability of our paper, some technical proofs of theorems and propositions will be deferred to Section 6. Some concluding remarks are made in Section 7.

2. Preliminaries on the Helmholtz Equation. Our multiscale algorithm relies on an in-depth understanding of the solution space of (1.1). To achieve this, we first present several analytic results for (1.1), which will serve as preliminaries for our subsequent discussions. We cover the weak formulation, the well-posedness of the equation, the stability estimates of the solution, and C^α estimates.

2.1. Notations. We use $H^1(\Omega)$ to denote the standard complex Sobolev space in Ω , containing L^2 functions with L^2 first order derivatives. We write $(u, v)_D := \int_D u \bar{v}$ for any domain D . We use C as a generic constant, and its value can change from place to place; however, we will state explicitly the parameters that this constant may or may not depend on.

2.2. Analytic Results. For the model problem (1.1), we consider the complex Sobolev space $\mathcal{H}(\Omega) := \{u \in H^1(\Omega) : u|_{\Gamma_D} = 0\}$ in which functions have zero trace on the Dirichlet boundary. This space is equipped with the norm $\|\cdot\|_{\mathcal{H}(\Omega)}$ such that

$$\|u\|_{\mathcal{H}(\Omega)} := \int_{\Omega} A |\nabla u|^2 + k^2 V^2 |u|^2.$$

The dual space of $\mathcal{H}(\Omega)$ is denoted by $\mathcal{H}^{-1}(\Omega)$ equipped with the norm $\|\cdot\|_{\mathcal{H}^{-1}(\Omega)}$; by definition one has

$$\|f\|_{\mathcal{H}^{-1}(\Omega)} := \sup_{v \in \mathcal{H}(\Omega)} \frac{(f, v)_{\Omega}}{\|v\|_{\mathcal{H}(\Omega)}}.$$

Now, we present several analytic results pertaining to the Helmholtz equation (1.1).

Weak formulation. The weak formulation of (1.1) is given by

$$(2.1) \quad a(u, v) := (A \nabla u, \nabla v)_{\Omega} - k^2 (V^2 u, v)_{\Omega} - (T_k u, v)_{\Gamma_N \cup \Gamma_R} = (f, v)_{\Omega}, \quad \forall v \in \mathcal{H}(\Omega).$$

Continuity estimate. By the Cauchy-Schwarz and trace inequalities (see Lemma 3.1 of [26]), the sesquilinear form $a(\cdot, \cdot)$ is bounded on $\mathcal{H}(\Omega)$ with a constant C_c independent of k , i.e., for any $u, v \in \mathcal{H}(\Omega)$, one has the continuity estimate:

$$(2.2) \quad |a(u, v)| \leq C_c \|u\|_{\mathcal{H}(\Omega)} \|v\|_{\mathcal{H}(\Omega)}.$$

Well-posedness and stability. If Γ_R has positive $d - 1$ dimensional measure, then under some mild conditions (see Assumption 2.3 and Theorem 2.4 in [17]), problem (2.1) admits a unique solution given the right hand side $f \in L^2(\Omega)$. We will assume these conditions. Let the solution operator be N_k , so that $u = N_k f$. Under the same conditions, this operator is stable (Theorem 2.4 in [17]) in the sense that

$$(2.3) \quad C_{\text{stab}}(k) := \sup_{f \in L^2(\Omega) \setminus \{0\}} \frac{\|N_k f\|_{\mathcal{H}(\Omega)}}{\|f\|_{L^2(\Omega)}} < \infty.$$

To avoid getting into detailed discussions of these assumptions and for simplicity of presentation, we will base most of our arguments on assuming (2.3) holds.

The stability constant $C_{\text{stab}}(k)$ will depend on k in general, and obtaining an explicit characterization of this dependence has been a hard task; see [4, 5, 18, 28, 37]. A prevalent and reasonable assumption on the constant is that of polynomial growth, namely $C_{\text{stab}}(k) \leq C(1 + k^\gamma)$ for some constants γ and C ; see for example [24]. We are not going into detailed discussions on this assumption here, while we mention that the final error estimate of our numerical solution in this paper will depend on $C_{\text{stab}}(k)$

explicitly; thus, those estimates on $C_{\text{stab}}(k)$ in the literature can be readily applied to our context.

In addition, stability for $f \in L^2(\Omega)$ can yield well-posedness and stability for $f \in \mathcal{H}^{-1}(\Omega)$. According to Lemma 2.1 in [34] and also [12], one has

$$(2.4) \quad \sup_{f \in \mathcal{H}^{-1}(\Omega) \setminus \{0\}} \frac{\|N_k f\|_{\mathcal{H}(\Omega)}}{\|f\|_{\mathcal{H}^{-1}(\Omega)}} \leq k C_{\text{stab}}(k).$$

Adjoint problems. Due to the presence of the Robin boundary condition, $a(\cdot, \cdot)$ is not Hermitian. Its adjoint sesquilinear form is defined as $a^*(u, v) = \overline{a(v, u)}$. The adjoint problem for (2.1) is given by $a^*(u, v) = (f, v)_\Omega$ for any $v \in \mathcal{H}(\Omega)$. It also corresponds to the following PDE:

$$\begin{cases} -\nabla \cdot (A \nabla u) - k^2 V^2 u = f, & \text{on } \Omega \\ u = 0, & \text{in } \Gamma_D \\ A \nabla u \cdot \nu = T_k^* u, & \text{on } \Gamma_N \cup \Gamma_R, \end{cases}$$

where $T_k^* u := \overline{T_k u} = -T_k u$. The adjoint solution operator is denoted by N_k^* . One can readily check that $N_k^* \overline{f} = \overline{N_k f}$. Therefore, the adjoint problem admits the same stability constant as the original problem; namely it holds

$$C_{\text{stab}}(k) = \sup_{f \in L^2(\Omega) \setminus \{0\}} \frac{\|N_k^* f\|_{\mathcal{H}(\Omega)}}{\|f\|_{L^2(\Omega)}} < \infty.$$

The adjoint problem will play valuable roles when we analyze the convergence property of our multiscale methods for the Helmholtz equation.

C^α regularity. We will need the C^α estimates of the solution in order to demonstrate the theoretical properties of our multiscale methods.

PROPOSITION 2.1. *Suppose $d \leq 3$ and (2.3) holds. If $f \in L^2(\Omega)$, then the solution $u \in C^\alpha(\Omega)$ for some $\alpha \in (0, 1)$.*

We defer the proof of this proposition to Subsection 6.1.

We have presented several critical analytic results for the Helmholtz equation. Based on these results, we are now ready to study the solution space of (1.1) in the next section. The key is a coarse-fine scale decomposition of the solution space, which will play an essential role in designing our multiscale algorithms.

3. Coarse-Fine Scale Decomposition. In this section, we develop a coarse-fine scale operator-adapted decomposition of the solution space. This decomposition is adaptive to the mesh structure, and a mesh of size $H = O(1/k)$ suffices to make this coarse-fine scale decomposition well defined. We discuss the setting of the mesh structure in Subsection 3.1, followed by introducing the coarse-fine scale decomposition in Subsection 3.2. In Subsection 3.3 we show the fine scale part is local and small up to $O(H)$ in the $\mathcal{H}(\Omega)$ norm. In Subsection 3.4 we show the coarse-scale component can be approximated via local edge basis functions in a nearly exponentially convergent manner.

3.1. Mesh Structure. We begin by discussing related concepts of the mesh structure. The focus here is on $d = 2$ while remarks on generalization to $d \geq 3$ will be given in Section 7. In the mesh structure, we discuss two dimensional elements in Subsection 3.1.1, one dimension edges and zero dimensional nodes, and their neighborhood in Subsection 3.1.2. See also Figure 3.1 for illustrations.

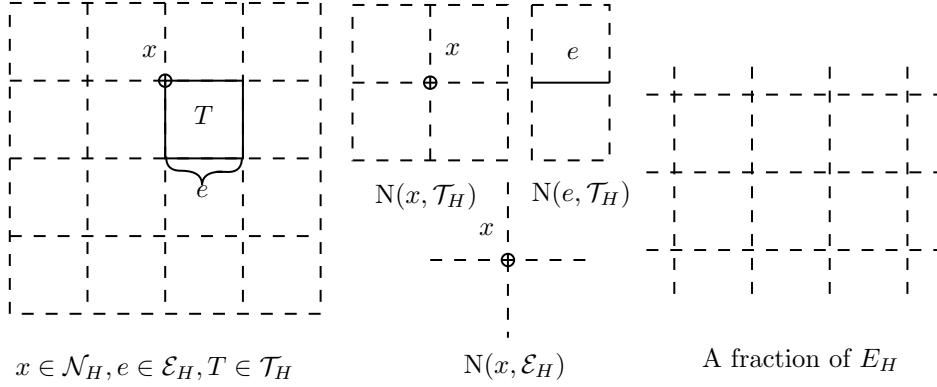


FIG. 3.1. Geometry of the mesh

3.1.1. Elements. We consider a shape regular and uniform partition of the domain Ω into finite elements, such as triangles and quadrilaterals. The collection of elements is denoted by $\mathcal{T}_H = \{T_1, T_2, \dots, T_r\}$; we adopt the convention that each T is an open set.

The mesh size is H , i.e., $\max_{T \in \mathcal{T}_H} \text{diam}(T) = H$. The uniformity of the mesh implies $\min_{T \in \mathcal{T}_H} \text{diam}(T) \geq c_0 H$ for some $0 < c_0 \leq 1$ that is independent of H and T . The shape regular property implies there is a constant $c_1 > 0$ independent of H and T , such that $\max_{T \in \mathcal{T}_H} \text{diam}(T)^d / |T| \leq c_1$, where $|T|$ is the volume of T .

In this mesh, by using a scaling argument, the following Poincaré inequality will hold uniformly for $T \in \mathcal{T}_H$. This inequality will be used frequently later.

PROPOSITION 3.1 (The Poincaré inequality). *For any $T \in \mathcal{T}_H$ and a function $v \in H^1(T)$ that vanishes on one of the edges of T , it holds that*

$$(3.1) \quad \|v\|_{L^2(T)} \leq C_P H \|\nabla v\|_{L^2(T)},$$

where C_P depends on c_0, c_1 and d .

3.1.2. Nodes, Edges and Their Neighbors. Let $\mathcal{N}_H = \{x_1, x_2, \dots, x_p\}$ be the collection of interior nodes, and $\mathcal{E}_H = \{e_1, e_2, \dots, e_q\}$ be the collection of edges except those fully on the boundary of Ω . An edge $e \in \mathcal{E}_H$ is defined such that there exists two different elements T_i, T_j with $e = \overline{T_i} \cap \overline{T_j}$ that has co-dimension 1 in \mathbb{R}^d . We will use $E_H = \bigcup_{e \in \mathcal{E}_H} e \subset \Omega$ to denote the edges as a whole set.

We use the symbol \sim to describe the neighbourhood between nodes, edges and elements. More precisely, if we consider a node $x \in \mathcal{N}_H$, an edge $e \in \mathcal{E}_H$, and an element $T \in \mathcal{T}_H$, then, (1) $x \sim e$ denotes $x \in e$; (2) $e \sim T$ denotes $e \subset \overline{T}$; (3) $x \sim T$ denotes $x \in \overline{T}$. The relationship \sim is symmetric.

We use $N(\cdot, \cdot)$ to describe the union of neighbors as a set. For example, $N(x, \mathcal{E}_H) = \bigcup \{e \in \mathcal{E}_H : e \sim x\} \subset E_H$, $N(x, \mathcal{T}_H) = \bigcup \{T \in \mathcal{T}_H : T \sim x\} \subset \Omega$, and $N(e, \mathcal{T}_H) = \bigcup \{T \in \mathcal{T}_H : T \sim e\} \subset \Omega$.

3.2. Decomposition of Solution Space. With the mesh structure defined, we now discuss the coarse-fine scale decomposition of the solution space. We first discuss decomposition in the local element T in Subsection 3.2.1 and then the global decomposition in Subsection 3.2.2.

3.2.1. Local decomposition. A crucial requirement for the decomposition to be well defined is that the mesh size is order $O(1/k)$; see Assumption 1. As we will see

later, this bound on H ensures that local Helmholtz problems in each element have properties that are similar to those of elliptic problems; thus, techniques in elliptic equations can then be applied.

ASSUMPTION 1. *The mesh size satisfies $H \leq A_{\min}^{1/2}/(\sqrt{2}C_P V_{\max} k)$, where C_P is the constant in Proposition 3.1.*

Given Assumption 1, we decompose² u into two parts $u = u_T^h + u_T^b$ in each element $T \in \mathcal{T}_H$. The two components satisfy:

$$(3.2) \quad \begin{cases} -\nabla \cdot (A \nabla u_T^h) - k^2 V^2 u_T^h = 0, & \text{in } T \\ u_T^h = u, & \text{on } \partial T \setminus (\Gamma_N \cup \Gamma_R) \\ A \nabla u_T^h \cdot \nu = T_k u_T^h, & \text{on } \partial T \cap (\Gamma_N \cup \Gamma_R), \\ -\nabla \cdot (A \nabla u_T^b) - k^2 V^2 u_T^b = f, & \text{in } T \\ u_T^b = 0, & \text{on } \partial T \setminus (\Gamma_N \cup \Gamma_R) \\ A \nabla u_T^b \cdot \nu = T_k u_T^b, & \text{on } \partial T \cap (\Gamma_N \cup \Gamma_R). \end{cases}$$

In short, the part u_T^h incorporates the boundary value of u , while u_T^b contains information of the right hand side. Both equations in (3.2) should be understood in the standard weak sense using the following local sesquilinear form $a_T(\cdot, \cdot)$ in T :

$$(3.3) \quad a_T(v, w) := (A \nabla v, \nabla w)_T - k^2 (V^2 v, w)_T - (T_k v, w)_{\partial T \cap (\Gamma_N \cup \Gamma_R)} \quad \text{for } v, w \in \mathcal{H}(T),$$

where $\mathcal{H}(T) := \mathcal{H}(\Omega)|_T$, the restriction of $\mathcal{H}(\Omega)$ in the domain T . The well-posedness of the two problems is due to the following proposition:

PROPOSITION 3.2. *Under Assumption 1, for $v \in \mathcal{H}(T)$ that vanishes on one of the edges of T , the corresponding sesquilinear form is coercive such that*

$$\Re a_T(v, v) \geq \frac{1}{2} \|A^{1/2} \nabla v\|_{L^2(T)}^2.$$

Proof. Using the Poincaré inequality (3.1) and Assumption 1, we get

$$(3.4) \quad \begin{aligned} \Re a_T(v, v) &= \|A^{1/2} \nabla v\|_{L^2(T)}^2 - \|k V v\|_{L^2(T)}^2 \\ &\geq (1 - C_P^2 H^2 k^2 V_{\max}^2 A_{\min}^{-1}) \|A^{1/2} \nabla v\|_{L^2(T)}^2 \geq \frac{1}{2} \|A^{1/2} \nabla v\|_{L^2(T)}^2. \end{aligned} \quad \square$$

Since both equations in (3.2) contain Dirichlet's boundary condition on at least one of the edges of T , the coercivity implied by Proposition 3.2 suffices for the well-posedness. Consequently, the solutions u_T^h and u_T^b are well-defined.

Remark 3.3. An important property is that u_T^h is “orthogonal” to u_T^b in T with respect to the local sesquilinear form $a_T(\cdot, \cdot)$ in T , in the sense of $a_T(u_T^h, u_T^b) = 0$, according to the weak form of the equation. Note that we might not have $a_T(u_T^b, u_T^h) = 0$ for T near the boundary (i.e., $\partial T \cap (\Gamma_N \cup \Gamma_R) \neq \emptyset$) due to the fact that $a_T(\cdot, \cdot)$ is not Hermitian here.

3.2.2. Global decomposition. In this subsection, we define a global decomposition $u = u^b + u^h$, such that for each T , it holds that $u^h(x) = u_T^h(x)$ and $u^b(x) = u_T^b(x)$

²This decomposition is inspired by that in the elliptic case [7].

when $x \in T$. Both u^h and u^b are well-defined and belong to $\mathcal{H}(\Omega)$ due to the continuity across edges. Here, the component u_T^h (resp. u^h) is called the local (resp. global) *Helmholtz-harmonic part* and u_T^b (resp. u^b) is the local (resp. global) *bubble part*, of the solution u .

We further introduce the function space for the Helmholtz-harmonic part

$$(3.5) \quad V^h := \{v \in \mathcal{H}(\Omega) : -\nabla \cdot (A\nabla v) - k^2 V^2 v = 0 \text{ in each } T \in \mathcal{T}_H, \\ A\nabla v \cdot \nu = T_k v, \text{ on } \Gamma_N \cup \Gamma_R\},$$

so that $u^h \in V^h$, and the space for the bubble part

$$(3.6) \quad V^b := \{v \in \mathcal{H}(\Omega) : v = 0 \text{ on } E_H\},$$

such that $u^b \in V^b$. In this way, the solution space of (1.1) can be decomposed to $V^h + V^b$. Furthermore, for any $v \in V^h$ and $w \in V^b$, it holds that $a(v, w) = 0$ by summing up local sesquilinear forms $a_T(\cdot, \cdot)$ and using Remark 3.3.

We will treat V^b as the fine scale or microscopic space, and refer to V^h as the coarse scale or macroscopic space. The idea of our multiscale framework is to compute the two parts separately by exploring their own structures.

In the next two subsections, we will study the computational properties of $u^h \in V^h$ and $u^b \in V^b$, respectively. These properties serve as the cornerstone of designing our multiscale algorithm.

3.3. Local and Small Bubble Part. In this subsection, we analyze the bubble part u^b . This part depends locally on f in each T . Thus, it can be computed efficiently in a parallel manner. Moreover, it is small and can be ignored if the target accuracy is of $O(H)$; see Proposition 3.4.

PROPOSITION 3.4. *Under Assumption 1, it holds that*

$$(3.7) \quad \|u^b\|_{\mathcal{H}(\Omega)} \leq \frac{3C_P}{A_{\min}^{1/2}} H \|f\|_{L^2(\Omega)}.$$

Proof. By definition, inside each patch T , it holds that $a_T(u^b, u^b) = (f, u^b)_T$. The coercive estimate in (3.4) implies the inequality $\|kVu^b\|_{L^2(T)}^2 \leq \frac{1}{2} \|A^{1/2} \nabla u^b\|_{L^2(T)}^2$. Using the estimate, we get

$$\begin{aligned} \Re a_T(u^b, u^b) &= \|A^{1/2} \nabla u^b\|_{L^2(T)}^2 - \|kVu^b\|_{L^2(T)}^2 \\ &\geq \frac{1}{3} (\|A^{1/2} \nabla u^b\|_{L^2(T)}^2 + \|kVu^b\|_{L^2(T)}^2) = \frac{1}{3} \|u^b\|_{\mathcal{H}(T)}^2. \end{aligned}$$

Combining the above estimate with the Cauchy-Schwarz inequality, we arrive at

$$\|u^b\|_{\mathcal{H}(T)}^2 \leq 3 \Re a_T(u^b, u^b) = 3(f, u^b)_T \leq 3 \|f\|_{L^2(T)} \|u^b\|_{L^2(T)}.$$

Meanwhile, by the Poincaré inequality (3.1), we get

$$\|u^b\|_{L^2(T)} \leq C_P H \|\nabla u^b\|_{L^2(T)} \leq \frac{C_P H}{A_{\min}^{1/2}} \|u^b\|_{\mathcal{H}(T)}.$$

Combining all the above inequalities gives $\|u^b\|_{\mathcal{H}(T)} \leq 3(C_P H / A_{\min}^{1/2}) \|f\|_{L^2(T)}$ for each element T . Summing them up for all elements T yields the desired conclusion. \square

3.4. Low Complexity of the Helmholtz-Harmonic Part. Now, we turn to the study of the Helmholtz-harmonic part u^h . The goal is to show that u^h can be approximated via local basis functions in an exponentially efficient manner. To achieve this, our approximation framework³ contains three steps: (1) reducing approximation of u^h to that of edge functions in Subsection 3.4.1; (2) localizing the approximation to every single edge in Subsection 3.4.2; and (3) realizing local approximation via oversampling and SVD in Subsection 3.4.3. Combining all these three steps, we establish the low complexity in approximation of u^h in Subsection 3.4.4.

3.4.1. Approximation via Edge Functions. We start with the first step of approximating u^h . By definition, u^h belongs to V^h . A key observation is that any function in V^h is determined entirely by its value on the edge set E_H . Thus, define

$$\tilde{V}^h := \{\tilde{\psi} : E_H \rightarrow \mathbb{R}, \text{ there exists a function } \psi \in V^h, \text{ such that } \tilde{\psi} = \psi|_{E_H}\};$$

then, there is a one to one correspondence $\tilde{\psi} \in \tilde{V}^h \leftrightarrow \psi \in V^h$. More precisely, in each T , it holds that

$$(3.8) \quad \begin{cases} -\nabla \cdot (A \nabla \psi) - k^2 V^2 \psi = 0, & \text{in } T \\ \psi = \tilde{\psi}, & \text{on } \partial T \setminus (\Gamma_N \cup \Gamma_R) \\ A \nabla \psi \cdot \nu = T_k \tilde{\psi}, & \text{on } \partial T \cap (\Gamma_N \cup \Gamma_R). \end{cases}$$

Indeed, we have $\tilde{V}^h = H^{1/2}(E_H)$ by the trace theory. Using the above correspondence, approximating u^h is equivalent to approximating \tilde{u}^h , which is a function defined on edges.

Remark 3.5. In the remaining part of the article, we will frequently use the correspondence between V^h and \tilde{V}^h . Conventionally, when we write a tilde on the top of a function in V^h , it refers to its corresponding part in \tilde{V}^h .

3.4.2. Localization of Approximation. We discuss how to approximate the edge function \tilde{u}^h , whose domain is E_H , which is nonlocal. Since it is often preferable to have localized basis functions for approximation and numerical algorithms, our second step is to localize the task of approximating \tilde{u}^h to every single edge.

To achieve localization, we study the geometry of the edge set E_H first. Observing that different edges only communicate with each other along their shared nodes, we can use nodal interpolation to localize the approximation. More precisely, we proceed with the following steps:

1. Interpolation: for each node $x_i \in \mathcal{N}_H$, choose $\tilde{\psi}_i$ to be the piecewise linear tent function on E_H , satisfying $\tilde{\psi}_i(x_j) = \delta_{ij}$ for each $x_j \in \mathcal{N}_H$. This defines an interpolation operator for $v \in V^h \cap C(\Omega)$:

$$I_H v := \sum_{x_i \in \mathcal{N}_H} v(x_i) \tilde{\psi}_i(x).$$

Note that $\tilde{\psi}_i(x)$ is the same as the basis function constructed via the multi-scale finite element method (MsFEM [23]). The interpolation residual $v - I_H v$ vanishes on each $x_i \in \mathcal{N}_H$. Set⁴ $v = \tilde{u}^h$ and let $I_H \tilde{u}^h$ be one part of the approximation for \tilde{u}^h . Then, it remains to approximate the residue $\tilde{u}^h - I_H \tilde{u}^h$.

³It is similar to that in our previous work for elliptic equations [7].

⁴Note that we can apply I_H to \tilde{u}^h due to the C^α estimate of u in Proposition 2.1.

2. Localization: we wish to explore the fact that $\tilde{u}^h - I_H \tilde{u}^h$ vanishes on nodes to localize the subsequent approximation task. To achieve so, define $R_e \tilde{u}^h = P_e(\tilde{u}^h - I_H \tilde{u}^h) := (\tilde{u}^h - I_H \tilde{u}^h)|_e$. The goal is to find some basis functions on each e to approximate $R_e \tilde{u}^h$. To make this problem precise, we need to specify the function space of $R_e \tilde{u}^h$, and the norm for approximation. It turns out that the natural function space $R_e \tilde{u}^h$ is the Lions-Magenes space; see the following Proposition 3.6.

PROPOSITION 3.6. *Suppose $d \leq 3$, $f \in L^2(\Omega)$ and (2.3) holds. For each $e \in \mathcal{E}_H$, it holds that $R_e \tilde{u}^h \in H_{00}^{1/2}(e)$, the Lions-Magenes space which contains functions $v \in H^{1/2}(e)$ such that*

$$\frac{v(x)}{\text{dist}(x, \partial e)} \in L^2(e).$$

Here $\text{dist}(x, \partial e)$ is the Euclidean distance from x to the boundary of e .

It might seem unclear at this stage why we should consider such a complicated function space. In fact, this is related to the zero extension of functions. According to Chapter 33 of [38], $H_{00}^{1/2}(e)$ can also be characterized as the space of functions in $H^{1/2}(e)$, such that their zero extensions to E_H is still in $H^{1/2}(E_H)$. This is the key and in fact the only property that we will use for $H_{00}^{1/2}(e)$. The zero extension allows us to connect local approximation and global approximation. In the following we will not distinguish $\tilde{\psi} \in H_{00}^{1/2}(e)$ and its zero extension to E_H that belongs to $H^{1/2}(E_H)$.

For any function in $H_{00}^{1/2}(e)$, we define a norm to measure approximation accuracy.

DEFINITION 3.7. *The $\mathcal{H}^{1/2}(e)$ norm of a function $\tilde{\psi} \in H_{00}^{1/2}(e)$ is defined as:*

$$(3.9) \quad \|\tilde{\psi}\|_{\mathcal{H}^{1/2}(e)}^2 := \int_{\Omega} A|\nabla \psi|^2 + k^2|V\psi|^2,$$

where we have used the one to one correspondence $\tilde{\psi} \in \tilde{V}^h \leftrightarrow \psi \in V^h$.

The $\mathcal{H}^{1/2}(e)$ norm in Definition 3.7 is the natural one to consider here since eventually, we aim for approximation accuracy in the energy norm.

The following theorem is the cornerstone for the above localization strategy. It states that a local accuracy guarantee can be seamlessly coupled to form a global accuracy guarantee.

THEOREM 3.8 (Global error estimate). *Suppose for each edge e , there exists an edge function $\tilde{v}_e \in H_{00}^{1/2}(e)$ that satisfies*

$$(3.10) \quad \|R_e \tilde{u}^h - \tilde{v}_e\|_{\mathcal{H}^{1/2}(e)} \leq \epsilon_e.$$

Let $v_e \in V^h$ be the corresponding part of $\tilde{v}_e \in \tilde{V}^h$. Then, it holds that

$$(3.11) \quad \|u^h - I_H u^h - \sum_{e \in \mathcal{E}_H} v_e\|_{\mathcal{H}(\Omega)}^2 \leq C_{\text{mesh}} \sum_{e \in \mathcal{E}_H} \epsilon_e^2,$$

where C_{mesh} is a constant depending on the number of edges for the elements only, e.g., for quadrilateral mesh $C_{\text{mesh}} = 4$.

Given this theorem, to approximate u^h it suffices to find local edge basis functions that satisfy (3.10) for some desired ϵ_e . This is a localized task for each e .

The proofs for Propositions 3.6 and Theorem 3.8 are similar to that in the setting of elliptic equations [7]. However, for completeness, we will also present them here in Subsections 6.2 and 6.3.

3.4.3. Local Approximation via Oversampling. The last step of approximation is to find local edge basis functions for each e so that (3.10) is satisfied. In this subsection, we discuss how to achieve this via oversampling and SVD, which can yield exponentially decaying ϵ_e . The general idea is to explore the fact that for a coarse scale function, its behavior on e can be controlled very well by that in an oversampling domain due to the compactness property of the restriction operator.

More precisely, for a given edge e , consider an oversampling domain ω_e associated with the edge. In general, any domain containing e in the interior can serve as a candidate. Here, for simplicity of presentation and as an illustrative example, we set

$$(3.12) \quad \omega_e = \overline{\bigcup \{T \in \mathcal{T}_H : \bar{T} \cap e \neq \emptyset\}}.$$

For interior edges and edges connected to the boundary, an illustration of this choice (3.12) for a quadrilateral mesh is given in Figure 3.2.

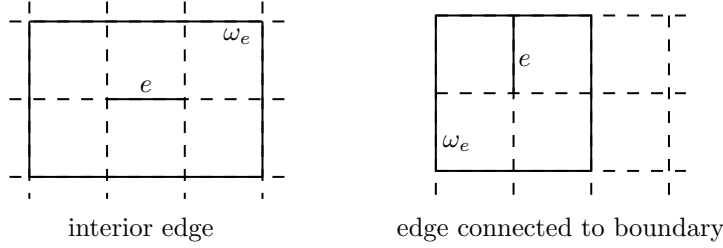


FIG. 3.2. Illustration of oversampling domains. On the right, we use an edge connected to the upper boundary as an illustrating example.

The key idea is to treat the residue $R_e \tilde{u}^h$ as a restriction of a coarse scale function in ω_e and explore the compactness property of such restriction operators. As a first step, we write

$$(3.13) \quad R_e \tilde{u}^h = R_e u = R_e u_{\omega_e}^h + R_e u_{\omega_e}^b,$$

where we decompose u in ω_e into its coarse and fine scale components, via (3.2) with T replaced by ω_e , and we shall use $u_{\omega_e}^h$ and $u_{\omega_e}^b$ to denote the corresponding local Helmholtz-harmonic and bubble part respectively. Then, to approximate $R_e \tilde{u}^h$, we could approximate the two terms in (3.13) separately. We will show that the first term can be approximated in an exponentially efficient manner due to a compactness property, and the second term can be computed locally and is very small.

Remark 3.9. One may ask whether the decomposition (3.13) in the oversampling domain is still well-defined. Indeed, similar to (3.1), we have a uniform Poincaré inequality for every ω_e : for any edge e and $H^1(\omega_e)$ function v vanishing on one of the four edge boundaries of ω_e , it holds that

$$(3.14) \quad \|v\|_{L^2(\omega_e)} \leq C'_P H \|\nabla v\|_{L^2(\omega_e)},$$

where C'_P is a constant that only depends on c_0, c_1, d and our choice of oversampling domain. For the particular choice (3.12), C'_P is a constant multiple of C_P ; without loss of generality we assume $C'_P \geq C_P$. Based on this observation, we will choose a small H so that Assumption 2 holds, which guarantees that local Helmholtz operators in the oversampling domain behave in a manner similar to that of elliptic case; this is similar to Proposition 3.2.

ASSUMPTION 2. *The mesh size satisfies $H \leq A_{\min}^{1/2}/(\sqrt{2}C'_P V_{\max} k)$, where C'_P is the constant in (3.14).*

Note that Assumption 2 implies Assumption 1. Now, we discuss in detail how to deal with the two terms in (3.13).

1. For the first term, we consider the following function space in ω_e :

$$(3.15) \quad \begin{aligned} U(\omega_e) := \{v \in \mathcal{H}(\omega_e) : -\nabla \cdot (A\nabla v) - k^2 V^2 v = 0, \text{ in } \omega_e \\ A\nabla v \cdot \nu = T_k v, \text{ on } (\Gamma_N \cup \Gamma_R) \cap \partial\omega_e\}. \end{aligned}$$

By definition, $u_{\omega_e}^h$ belongs to $U(\omega_e)$. Under Assumption 2, $(U(\omega_e), \|\cdot\|_{\mathcal{H}(\omega_e)})$ is a Hilbert space, since the Helmholtz operator in ω_e is elliptic. Then, by abuse of notation, consider the operator

$$R_e : (U(\omega_e), \|\cdot\|_{\mathcal{H}(\omega_e)}) \rightarrow (H_{00}^{1/2}(e), \|\cdot\|_{\mathcal{H}^{1/2}(e)}),$$

such that $R_e v = P_e(v - I_H v)$ for $v \in U(\omega_e)$. A critical property is that the singular values of R_e decay nearly exponentially fast; see Theorem 3.10. Its proof is deferred to Subsection 6.4.

THEOREM 3.10. *Under Assumption 2, the operator R_e is compact for each $e \in \mathcal{E}_H$. Denote the pairs of its left singular vectors and singular values by $\{\tilde{v}_{m,e}, \lambda_{m,e}\}_{m \in \mathbb{N}}$, where $\tilde{v}_{m,e} \in H_{00}^{1/2}(e)$ and the sequence $\{\lambda_{m,e}\}_{m \in \mathbb{N}}$ is in a descending order. Then, for any $\epsilon > 0$, it holds that*

$$(3.16) \quad \lambda_{m,e} \leq C_\epsilon \exp\left(-m^{(\frac{1}{d+1}-\epsilon)}\right),$$

where C_ϵ is a constant that is independent of k, H and may depend on ϵ, d and the mesh parameters c_0, c_1 .

We discuss the implication of this theorem. By definition of singular values, if we set $W_{m,e} = \text{span}\{\tilde{v}_{k,e}\}_{k=1}^{m-1}$, then Theorem 3.10 implies that

$$(3.17) \quad \min_{\tilde{v}_e \in W_{m,e}} \|R_e v - \tilde{v}_e\|_{\mathcal{H}^{1/2}(e)} \leq C_\epsilon \exp\left(-m^{(\frac{1}{d+1}-\epsilon)}\right) \|v\|_{\mathcal{H}(\omega_e)}.$$

Applying this result to $v = u_{\omega_e}^h \in U(\omega_e)$ leads to

$$(3.18) \quad \min_{\tilde{v}_e \in W_{m,e}} \|R_e u_{\omega_e}^h - \tilde{v}_e\|_{\mathcal{H}^{1/2}(e)} \leq C_\epsilon \exp\left(-m^{(\frac{1}{d+1}-\epsilon)}\right) \|u_{\omega_e}^h\|_{\mathcal{H}(\omega_e)}.$$

Thus, there is a nearly exponential efficiency in approximating the first term $R_e u_{\omega_e}^h$.

2. For the second term in (3.13), the oversampling bubble part $u_{\omega_e}^b$ can be efficiently computed by solving local Helmholtz problems. Moreover, under Assumption 2 this term is small in the $\mathcal{H}(\Omega)$ norm as shown in the following proposition.

PROPOSITION 3.11. *Under Assumption 2, for each $e \in \mathcal{E}_H$ the following estimate holds for the oversampling bubble part:*

$$\|R_e u_{\omega_e}^b\|_{\mathcal{H}^{1/2}(e)} \leq CH \|f\|_{L^2(\omega_e)},$$

where C is a constant independent of k and H .

The proof is deferred to Subsection 6.5.

Define the following space of edge basis functions:

$$\tilde{V}_{H,m,e}^{(1)} := \text{span} \{W_{m,e} \cup R_e u_{\omega_e}^b\}.$$

In practice, this space can be computed locally by a SVD of R_e and by solving a local equation. Due to (3.13) and (3.18), we have the following error estimate on each e :

$$(3.19) \quad \min_{\tilde{v}_e \in \tilde{V}_{H,m,e}^{(1)}} \|R_e u^h - \tilde{v}_e\|_{\mathcal{H}^{1/2}(e)} \leq C_\epsilon \exp\left(-m^{(\frac{1}{d+1}-\epsilon)}\right) \|u_{\omega_e}^h\|_{\mathcal{H}(\omega_e)}.$$

3.4.4. Low Complexity in Approximation. Finally, define the collection of edge basis functions

$$\tilde{V}_{H,m}^{(1)} = \text{span} \left\{ \bigcup_e \tilde{V}_{H,m,e}^{(1)} \right\},$$

and denote by $\tilde{V}_H^{(0)}$ the span of the nodal interpolation basis used earlier, i.e. $\tilde{V}_H^{(0)} := \text{span} \{\tilde{\psi}_i\}$. Define the overall edge approximation $\tilde{V}_{H,m} = \text{span} \{\tilde{V}_H^{(0)} \cup \tilde{V}_{H,m}^{(1)}\}$. Let $V_{H,m} \subset V^h$ be the corresponding part of $\tilde{V}_{H,m} \subset \tilde{V}^h$, via (3.8). Then, using (3.19) and Theorem 3.8, we get an nearly exponentially decaying error estimate for approximating u^h ; see Theorem 3.12.

THEOREM 3.12. *Under Assumption 2 and (2.3), it holds that*

$$\min_{v \in V_{H,m}} \|u^h - v\|_{\mathcal{H}(\Omega)} \leq C(C_{\text{stab}}(k) + H) \exp\left(-m^{(\frac{1}{d+1}-\epsilon)}\right) \|f\|_{L^2(\Omega)},$$

where C is a generic constant independent of k, m, H .

Proof. By Theorem 3.10 and the global error estimate in Theorem 3.8, we get

$$(3.20) \quad \min_{v \in V_{H,m}} \|u^h - v\|_{\mathcal{H}(\Omega)}^2 \leq C_{\text{mesh}} C_\epsilon^2 \exp\left(-2m^{(\frac{1}{d+1}-\epsilon)}\right) \sum_{e \in \mathcal{E}_H} \|u_{\omega_e}^h\|_{\mathcal{H}(\omega_e)}^2.$$

Due to Assumption 2, we have the elliptic estimate for the oversampling bubble part

$$(3.21) \quad \|u_{\omega_e}^b\|_{\mathcal{H}(\omega_e)} \leq \frac{3C_P'}{A_{\min}^{1/2}} H \|f\|_{L^2(\omega_e)}.$$

This is similar to Proposition 3.4, which is a consequence of Assumption 1. Then, using $u_{\omega_e}^h = u - u_{\omega_e}^b$, it follows that

$$(3.22) \quad \|u_{\omega_e}^h\|_{\mathcal{H}(\omega_e)}^2 \leq 2(\|u\|_{\mathcal{H}(\omega_e)}^2 + \|u_{\omega_e}^b\|_{\mathcal{H}(\omega_e)}^2) \leq \frac{18C_P'^2}{A_{\min}} H^2 \|f\|_{L^2(\omega_e)}^2 + 2\|u\|_{\mathcal{H}(\omega_e)}^2.$$

Note that by our choice of oversampling domains, every element T can only be covered by $\{\omega_e\}_{e \in \mathcal{E}_H}$ at most C_1 times for a fixed C_1 . Therefore it holds that

$$(3.23) \quad \sum_{e \in \mathcal{E}_H} \|f\|_{L^2(\omega_e)}^2 \leq C_1 \|f\|_{L^2(\Omega)}^2,$$

as well as

$$(3.24) \quad \sum_{e \in \mathcal{E}_H} \|u_{\omega_e}\|_{\mathcal{H}(\omega_e)}^2 \leq C_1 \|u\|_{\mathcal{H}(\Omega)}^2 \leq C_1 C_{\text{stab}}^2(k) \|f\|_{L^2(\Omega)}^2,$$

where the last inequality is due to the *a priori* estimate (2.3). Combining (3.20), (3.23), (3.23) and (3.24) completes the proof. \square

Clearly, Theorem 3.12 implies the low complexity property of the part u^h . Each edge contains at most m basis functions, so the space $V_{H,m}$ is of dimension $O(m/H^2)$, while the approximation accuracy is of order $\exp\left(-m^{(\frac{1}{d+1}-\epsilon)}\right)$. We will use the space $V_{H,m}$ in our multiscale framework for approximating u^h .

4. The Multiscale Methods. In this section, we discuss the multiscale methods for solving (1.1), based on the coarse-fine scale decomposition established in the last section.

By the nature of a multiscale algorithm, we will handle the coarse part u^h and the fine part u^b separately. Conceptually, the locality and small magnitude of u^b implies it can be computed efficiently or ignored without influencing the accuracy much, and the low complexity of u^h indicates that we can use a Galerkin method with a small number of basis functions to approximate it accurately.

In Subsection 4.1, we outline our general multiscale computational framework. Depending on how the trial and test spaces in the Galerkin method are selected, we get two categories of algorithms, namely the Ritz-Galerkin approach and Petrov-Galerkin approach that we will make precise in Subsections 4.2 and 4.3, respectively.

4.1. The Multiscale Framework. The bubble part u^b is first computed locally. Given this part, we form an effective equation for u^h as

$$(4.1) \quad a(u^h, v) = (f, v)_\Omega - a(u^b, v),$$

for any $v \in \mathcal{H}(\Omega)$.

Remark 4.1. The right hand side in (4.1) can be seen as a bounded linear functional on $v \in \mathcal{H}(\Omega)$. By the estimate in (2.4), this equation for u^h (given fixed u^b) is well-posed.

Numerically, we solve the equation (4.1) for u^h using a Galerkin method. That is, we choose a trial space S and a test space S_{test} to find a numerical solution $u_S \in S$ that satisfies

$$(4.2) \quad a(u_S, v) = (f, v)_\Omega - a(u^b, v),$$

for any $v \in S_{\text{test}}$. If $S_{\text{test}} = S$, then it is called a Ritz-Galerkin method, otherwise it is a Petrov-Galerkin method. Here by the complex nature of the equation, we specifically refer to the choice $S_{\text{test}} = \overline{S}$ as the Petrov-Galerkin method.

In Subsection 4.2, we formulate our Ritz-Galerkin method and present theories for the well-posedness of the discrete problem, as well as the error estimate in both the energy norm and the L^2 norm. In Subsection 4.3, we discuss the Petrov-Galerkin method, which is more straightforward and appears more convenient in practical computation.

4.2. The Ritz-Galerkin Method. First, we establish a general strategy for analyzing the Ritz-Galerkin method in solving (4.1). We start with a definition of the approximation accuracy of S .

DEFINITION 4.2. For $S \subset V^h$, the approximation accuracy of S is defined as

$$(4.3) \quad \eta^h(S) := \sup_{f \in L^2(\Omega) \setminus \{0\}} \inf_{v \in S} \frac{\|u^h - v\|_{\mathcal{H}(\Omega)}}{\|f\|_{L^2(\Omega)}},$$

where u and f are related via the Helmholtz equation in (1.1).

For the Ritz-Galerkin method, it turns out that $\eta^h(S)$ is critical in analyzing the solution errors of u_S .

THEOREM 4.3. *Suppose (2.3) holds and $k\eta^h(S) \leq 1/(4C_c V_{\max})$ as well as $\bar{S} = S$. Then, the following statements hold for the Ritz-Galerkin method:*

1. *The Galerkin solution u_S is a quasi-optimal approximation in the sense that*

$$\begin{aligned} \|u^h - u_S\|_{\mathcal{H}(\Omega)} &\leq 2C_c \inf_{v \in S} \|u^h - v\|_{\mathcal{H}(\Omega)}, \\ \|u^h - u_S\|_{L^2(\Omega)} &\leq C_c \eta^h(S) \|u^h - u_S\|_{\mathcal{H}(\Omega)}. \end{aligned}$$

2. *The discrete problem satisfies the discrete inf-sup stability condition:*

$$\inf_{v \in S} \sup_{v' \in S \setminus \{0\}} \frac{|a(v, v')|}{\|v\|_{\mathcal{H}(\Omega)} \|v'\|_{\mathcal{H}(\Omega)}} \geq \frac{1}{2 + C_c^{-1} + 4kV_{\max}C_{\text{stab}}(k) + 6\sqrt{2}}.$$

Proof. Define $e_S = u^h - u_S \in V^h$. Take $\psi = N_k^*(e_S)$. It holds that

$$\|e_S\|_{L^2(\Omega)}^2 = a(e_S, \psi) = a(e_S, \psi - v - w),$$

for any $v \in S$ and $w \in V^b$, due to the property of the Galerkin solution and the one-direction orthogonality (see Remark 3.3) between V^h and V^b . Thus, using the boundness of $a(\cdot, \cdot)$, we obtain that

$$(4.4) \quad \|e_S\|_{L^2(\Omega)}^2 \leq C_c \|e_S\|_{\mathcal{H}(\Omega)} \|\psi - v - w\|_{\mathcal{H}(\Omega)} = C_c \|e_S\|_{\mathcal{H}(\Omega)} \|\bar{\psi} - \bar{v} - \bar{w}\|_{\mathcal{H}(\Omega)}.$$

As $\bar{\psi} = N_k \bar{e}_S$ according to the definition of the adjoint problem in Subsection 2.2, we can take $\bar{w} = (N_k \bar{e}_S)^b$ so that $\bar{\psi} - \bar{v} - \bar{w} = (N_k \bar{e}_S)^h - \bar{v}$. Using the fact that $S = \bar{S}$, the definition (4.3), the inequality (4.4) and taking infimum of v over S , we get

$$\|e_S\|_{L^2(\Omega)}^2 \leq C_c \|e_S\|_{\mathcal{H}(\Omega)} \cdot \eta^h(S) \|\bar{e}_S\|_{L^2(\Omega)},$$

which leads to the desired $L^2(\Omega)$ error estimate: $\|e_S\|_{L^2(\Omega)} \leq C_c \eta^h(S) \|e_S\|_{\mathcal{H}(\Omega)}$.

For the $\mathcal{H}(\Omega)$ error, the property of Galerkin's solution implies that for any $v \in S$, we have

$$\begin{aligned} \|e_S\|_{\mathcal{H}(\Omega)}^2 &= \Re a(e_S, e_S) + \{\|e_S\|_{\mathcal{H}(\Omega)}^2 - \Re a(e_S, e_S)\} \\ (4.5) \quad &= \Re a(e_S, u^h - v) + 2\|kV(x)e_S\|_{L^2(\Omega)}^2 + \Re(T_k e_S, e_S)_{\Gamma_N \cup \Gamma_R} \\ &\leq C_c \|e_S\|_{\mathcal{H}(\Omega)} \|u^h - v\|_{\mathcal{H}(\Omega)} + 2(kV_{\max}C_c \eta^h(S))^2 \|e_S\|_{\mathcal{H}(\Omega)}^2, \end{aligned}$$

where we have used the fact that $\Re(T_k e_S, e_S)_{\Gamma_N \cup \Gamma_R} \leq 0$ and the $L^2(\Omega)$ error estimate we established before.

By the assumption $k\eta^h(S) \leq 1/(4C_c V_{\max})$, the last term in (4.5) is bounded by $\frac{1}{2}\|e_S\|_{\mathcal{H}(\Omega)}^2$. Thus due to the arbitrariness of v , we arrive at

$$\|e_S\|_{\mathcal{H}(\Omega)} \leq 2C_c \inf_{v \in S} \|u^h - v\|_{\mathcal{H}(\Omega)}.$$

This completes the proof for the first part. Next, we move to the proof for the discrete inf-sup stability. For any $v \in S$, set $z = 2N_k^*(k^2 V^2 v) \in \mathcal{H}(\Omega)$ so that $a(v, z) = 2k^2(V^2 v, v)_\Omega$. Plugging v and $v + z$ into the sesquilinear form yields:

$$\begin{aligned} a(v, v + z) &= a(v, v) + a(v, z) \\ &= (A \nabla v, \nabla v)_\Omega - k^2(V^2 v, v)_\Omega - (T_k v, v)_{\Gamma_N \cup \Gamma_R} + a(v, z) \\ &= (A \nabla v, \nabla v)_\Omega + k^2(V^2 v, v)_\Omega - (T_k v, v)_{\Gamma_N \cup \Gamma_R} + a(v, z) - 2k^2(V^2 v, v)_\Omega \\ &= \|v\|_{\mathcal{H}(\Omega)}^2 - (T_k v, v)_{\Gamma_N \cup \Gamma_R}. \end{aligned}$$

By the definition of T_k , $\Re(T_k v, v)_{\Gamma_N \cup \Gamma_R} \leq 0$, so it holds that

$$\Re a(v, v + z) \geq \|v\|_{\mathcal{H}(\Omega)}^2.$$

Now, by the definition of the adjoint problem, we have $\bar{z} = 2N_k(k^2 V^2 \bar{v})$. We can decompose $\bar{z} = \bar{z}^h + \bar{z}^b$. Let $z_S \in S$ achieve the best approximation in (4.3) for $f = 2k^2 V^2 \bar{v}$, so that

$$(4.6) \quad \|\bar{z}^h - z_S\|_{\mathcal{H}(\Omega)} \leq 2\eta^h(S) \|k^2 V^2 \bar{v}\|_{L^2(\Omega)} \leq 2kV_{\max} \eta^h(S) \|v\|_{\mathcal{H}(\Omega)}.$$

Choose $v' = v + \bar{z}_S \in S$. We have

$$\begin{aligned} \Re a(v, v + \bar{z}_S) &= \Re a(v, v + z) - \Re a(v, z - \bar{z}_S - w) \\ &\geq \|v\|_{\mathcal{H}(\Omega)}^2 - C_c \|v\|_{\mathcal{H}(\Omega)} \|\bar{z} - z_S - \bar{w}\|_{\mathcal{H}(\Omega)}, \end{aligned}$$

for any $w \in V^b$. Take $\bar{w} = \bar{z}^b$ and use the bound in (4.6) to get

$$(4.7) \quad a(v, v + \bar{z}_S) \geq \|v\|_{\mathcal{H}(\Omega)}^2 (1 - 2C_c k V_{\max} \eta^h(S)).$$

Meanwhile, by a triangle inequality, we get

$$\|v + \bar{z}_S\|_{\mathcal{H}(\Omega)} \leq \|v\|_{\mathcal{H}(\Omega)} + \|z - \bar{z}_S - \bar{w}\|_{\mathcal{H}(\Omega)} + \|z\|_{\mathcal{H}(\Omega)} + \|\bar{w}\|_{\mathcal{H}(\Omega)}$$

By the stability estimate in (2.3), we have

$$\|z\|_{\mathcal{H}(\Omega)} \leq C_{\text{stab}}(k) \|2k^2 V^2 v\|_{L^2(\Omega)} \leq 2C_{\text{stab}}(k) k V_{\max} \|v\|_{\mathcal{H}(\Omega)},$$

and by the bound on the bubble part as in Proposition 3.4, it holds that

$$\|w\|_{\mathcal{H}(\Omega)} \leq \frac{3C_P}{A_{\min}^{1/2}} H \|2k^2 V^2 \bar{v}\|_{L^2(\Omega)} \leq \frac{6C_P}{A_{\min}^{1/2}} H k V_{\max} \|v\|_{\mathcal{H}(\Omega)} \leq 3\sqrt{2} \|v\|_{\mathcal{H}(\Omega)},$$

where in the last inequality we have used Assumption 1. Thus, we have

$$\|v + \bar{z}_S\|_{\mathcal{H}(\Omega)} \leq (1 + 2\eta^h(S) k V_{\max} + 2C_{\text{stab}}(k) k V_{\max} + 3\sqrt{2}) \|v\|_{\mathcal{H}(\Omega)}.$$

Therefore, we obtain

$$\begin{aligned} \sup_{v' \in S \setminus \{0\}} \frac{|a(v, v')|}{\|v\|_{\mathcal{H}(\Omega)} \|v'\|_{\mathcal{H}(\Omega)}} &\geq \frac{|a(v, v + \bar{z}_S)|}{\|v\|_{\mathcal{H}(\Omega)} \|v + \bar{z}_S\|_{\mathcal{H}(\Omega)}} \geq \frac{\Re a(v, v + \bar{z}_S)}{\|v\|_{\mathcal{H}(\Omega)} \|v + \bar{z}_S\|_{\mathcal{H}(\Omega)}} \\ &\geq \frac{(1 - 2\eta^h(S) C_c k V_{\max}) \|v\|_{\mathcal{H}(\Omega)}^2}{(1 + 2\eta^h(S) k V_{\max} + 2C_{\text{stab}}(k) k V_{\max} + 3\sqrt{2}) \|v\|_{\mathcal{H}(\Omega)}^2}. \end{aligned}$$

Using the assumption that $\eta^h(S) k V_{\max} \leq 1/(4C_c)$, we obtain the desired estimate. \square

This theorem implies that once $\eta^h(S)$ is small, the discrete problem is well-posed, and the Galerkin solution approximates the exact solution accurately.

Given Theorem 4.3, we can choose $S = V_{H,m} + \bar{V}_{H,m}$ where $V_{H,m}$ is defined in Theorem 3.12. Then, the following error estimate for the Galerkin solution holds:

THEOREM 4.4. *Suppose Assumption 2 and (2.3) hold, and*

$$Ck(C_{\text{stab}}(k) + H) \exp\left(-m^{\left(\frac{1}{d+1} - \epsilon\right)}\right) \leq 1/(4C_c V_{\max}),$$

where C is the constant in Theorem 3.12, then using $S = V_{H,m} + \overline{V_{H,m}}$ in the Ritz-Galerkin method leads to a solution u_S that satisfies

$$(4.8) \quad \begin{aligned} \|u^h - u_S\|_{\mathcal{H}(\Omega)} &\leq 2C_c C(C_{\text{stab}}(k) + H) \exp\left(-m^{(\frac{1}{d+1}-\epsilon)}\right) \|f\|_{L^2(\Omega)}, \\ \|u^h - u_S\|_{L^2(\Omega)} &\leq 2(C_c C)^2 (C_{\text{stab}}(k) + H)^2 \exp\left(-2m^{(\frac{1}{d+1}-\epsilon)}\right) \|f\|_{L^2(\Omega)}. \end{aligned}$$

Proof. By Theorem 3.12, $\eta^h(S) \leq C(C_{\text{stab}}(k) + H) \exp\left(-m^{(\frac{1}{d+1}-\epsilon)}\right)$. By invoking Theorem 4.3, we complete the proof. \square

If $m \sim O(\log^{d+2}(kC_{\text{stab}}(k)))$ then the condition in Theorem 4.4 holds for some small ϵ , i.e. $\frac{1}{d+1} - \epsilon = \frac{1}{d+2}$. Further, if $C_{\text{stab}}(k) \leq C(1 + k^\gamma)$ for some constants γ and C , then $m \sim \log^{d+2}(k)$ suffices for this condition. This implies that once m is moderately large, i.e., logarithmically in k , the nearly exponential convergence of the Galerkin solution shown in Theorem 4.4 will become effective.

We provide several additional remarks of the Ritz-Galerkin method below.

Remark 4.5. In the Ritz-Galerkin method, the trial and test spaces are $S = V_{H,m} + \overline{V_{H,m}}$. One can intuitively understand that $V_{H,m}$ is needed to represent the desired solution, and $\overline{V_{H,m}}$ is used for the approximation of the adjoint problem, which is required in the numerical analysis of the Helmholtz equation. There can be a lot of overlap between $V_{H,m}$ and $\overline{V_{H,m}}$: on each interior edge, since the singular vectors of R_e are real, these edge basis functions are real-valued. Thus, $V_{H,m}$ and $\overline{V_{H,m}}$ can only differ on the edges connected to the boundary, where the presence of the Robin boundary condition makes the operator non-Hermitian.

Remark 4.6. Combining (4.8) with the local computation of the bubble part will yield the overall error estimate for u , which is nearly exponentially convergent. If $R_e u_{\omega_e}^b$ is not computed, then the overall error will be at most $O(H)$ in the $\mathcal{H}(\Omega)$ norm, and $O(H^2)$ in the L^2 norm.

Remark 4.7. In (4.1), we need to additionally compute the part $a(u^b, v)$ for each basis function v . The computational burden is effectively low. Indeed, for each inner edge, we have $a(u^b, v) = \overline{a(v, u^b)} = 0$ for a basis function v induced by this edge, due to the fact that this sesquilinear form is symmetric in the interior and the one-direction orthogonality between V^h and V^b . Thus, we only need to additionally compute $a(u^b, v)$ for v induced by edges connected to the boundary.

4.3. The Petrov-Galerkin Method. In this subsection, we introduce the Petrov-Galerkin method. We choose $S = V_{H,m}$ and $S_{\text{test}} = \overline{V_{H,m}}$. The following theorem bounds the $L^2(\Omega)$ error of the associated solution in terms of the $\mathcal{H}(\Omega)$ norm.

THEOREM 4.8. *Suppose Assumption 2 and (2.3) hold, and*

$$Ck(C_{\text{stab}}(k) + H) \exp\left(-m^{(\frac{1}{d+1}-\epsilon)}\right) \leq 1/(4C_c V_{\text{max}}),$$

where C is the constant in Theorem 3.12, then for the Petrov-Galerkin method with $S = V_{H,m}$ and $S_{\text{test}} = \overline{V_{H,m}}$, the solution u_S satisfies

$$(4.9) \quad \|u^h - u_S\|_{L^2(\Omega)} \leq 2C_c C(C_{\text{stab}}(k) + H) \exp\left(-m^{(\frac{1}{d+1}-\epsilon)}\right) \|u^h - u_S\|_{\mathcal{H}(\Omega)}.$$

Proof. Define $e_S = u^h - u_S \in V^h$. Take $\psi = N_k^*(e_S)$. Similar to the proof of Theorem 4.3 especially (4.4), we get

$$(4.10) \quad \|e_S\|_{L^2(\Omega)}^2 \leq C_c \|e_S\|_{\mathcal{H}(\Omega)} \|\bar{\psi} - \bar{v} - \bar{w}\|_{\mathcal{H}(\Omega)},$$

for any $v \in \overline{V_{H,m}}$ and $w \in V^b$. Choose $\bar{w} = (N_k \bar{e}_S)^b$ so that $\bar{\psi} - \bar{v} - \bar{w} = (N_k \bar{e}_S)^h - \bar{v}$. Based on the fact that $\bar{v} \in V_{H,m} = S$ and the definition of $\eta^h(S)$, we take the infimum over $\bar{v} \in S$ to get

$$\|e_S\|_{L^2(\Omega)}^2 \leq C_c \|e_S\|_{\mathcal{H}(\Omega)} \cdot \eta^h(S) \|\bar{e}_S\|_{L^2(\Omega)},$$

which implies that $\|u^h - u_S\|_{L^2(\Omega)} \leq C_c \eta^h(S) \|u^h - u_S\|_{\mathcal{H}(\Omega)}$. Note that the condition in the theorem leads to $\eta^h(S) \leq C(C_{\text{stab}}(k) + H) \exp\left(-m^{(\frac{1}{d+1}-\epsilon)}\right)$. Combining the above two estimates completes the proof. \square

Remark 4.9. The trial and test spaces in the Petrov-Galerkin method often have smaller dimensions than their Ritz-Galerkin counterpart, since we do not put the complex conjugate $\overline{V_{H,m}}$ in S . This can save computational efforts.

Remark 4.10. A main benefit of the Petrov-Galerkin method is that, equation (4.1) becomes $a(u_S, v) = (f, v)_\Omega$, due to the fact that $a(u^b, v) = a(\bar{v}, \bar{u}^b) = 0$, where $\bar{v} \in V_{H,m} \subset V^h$ and we have used the property $a(\bar{v}, w) = 0$ for any $w \in V^b$. Therefore, the effective equation for u^h is the same as the equation for u : we do not need to compute additional terms. Computations of u^h and u^b are automatically decoupled.

Remark 4.11. Our current theory does not address the stability of the discrete system and the $\mathcal{H}(\Omega)$ error estimate for the Petrov-Galerkin method. This is left for our future work. We note that our numerical experiments in the next section imply that these properties also hold for the Petrov-Galerkin method.

5. Numerical Experiments. In this section, we will outline and discuss our numerical algorithms in detail based on the established theoretical analysis. Several Helmholtz equations are solved using our algorithm, which confirm our theoretical results. We also consider some examples in which our theoretical assumptions are not satisfied. Even for these examples, our methods still give a nearly exponential rate of convergence. This provides further evidence for the robustness of our methods.

5.1. Set-up. We consider the domain $\Omega = [0, 1] \times [0, 1]$ and discretize it by a uniform two-level quadrilateral mesh; see a fraction of this mesh in Figure 5.1, where we also show an edge e and its oversampling domain ω_e in solid lines. The coarse and fine mesh sizes are denoted by H and h , respectively.

For a given Helmholtz equation, we compute the reference solution u_{ref} using the classical FEM on the fine mesh; with a sufficiently small h , it is reasonable to treat u_{ref} as the ground truth u .

The accuracy of a numerical solution u_{sol} is computed by comparing it with the reference solution u_{ref} on the fine mesh. The accuracy will be measured both in the L^2 norm and energy norm:

$$(5.1) \quad \begin{aligned} e_{L^2} &= \frac{\|u_{\text{ref}} - u_{\text{sol}}\|_{L^2(\Omega)}}{\|u_{\text{ref}}\|_{L^2(\Omega)}}, \\ e_{\mathcal{H}} &= \frac{\|u_{\text{ref}} - u_{\text{sol}}\|_{\mathcal{H}(\Omega)}}{\|u_{\text{ref}}\|_{\mathcal{H}}}. \end{aligned}$$

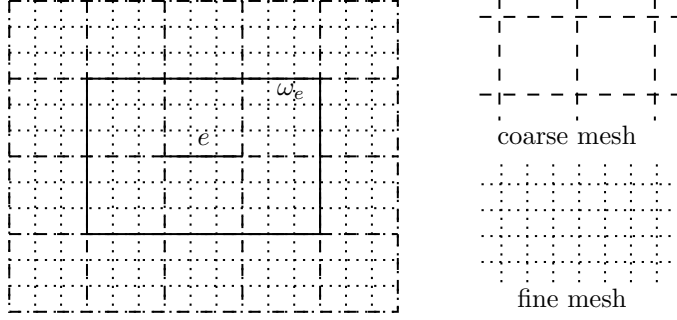


FIG. 5.1. Two level mesh: a fraction

5.2. Multiscale Algorithms. We outline our numerical algorithms for obtaining u_{sol} . There are offline and online stages, depending on whether the steps involve the information of the right hand side.

5.2.1. Offline Stage. For each edge $e \in \mathcal{E}_H$ and its associated oversampling domain ω_e , the key step in the offline stage is to construct the discretized version of the operator

$$R_e : (U(\omega_e), \|\cdot\|_{\mathcal{H}(\omega_e)}) \rightarrow (H_{00}^{1/2}(e), \|\cdot\|_{\mathcal{H}^{1/2}(e)}),$$

which is defined by $R_e v = (v - I_H v)|_e$. Here $U(\omega_e)$ is defined in (3.15), $\|\cdot\|_{\mathcal{H}(\omega_e)}$ is the energy norm in ω_e , while $H_{00}^{1/2}(e)$ is the Lion-Magenes space, and $\|\cdot\|_{\mathcal{H}^{1/2}(e)}$ is defined in (3.9).

We note that functions in $U(\omega_e)$ are fully determined by their traces on $\partial\omega_e \setminus (\Gamma_N \cup \Gamma_R)$. Thus, we can take the discretized matrix version of R_e as a linear mapping from Dirichlet's data on $\partial\omega_e \setminus (\Gamma_N \cup \Gamma_R)$ to the image of R_e , which contains functions on the edge e . The discretization of the $\|\cdot\|_{\mathcal{H}(\omega_e)}$ and $\|\cdot\|_{\mathcal{H}^{1/2}(e)}$ norms leads to positive definite matrices on the discretized domains $\partial\omega_e \setminus (\Gamma_N \cup \Gamma_R)$ and e . To obtain these positive definite matrices, we construct the Helmholtz-harmonic extension operators both on e and $\partial\omega_e \setminus (\Gamma_N \cup \Gamma_R)$, which maps boundary data to the Helmholtz-harmonic function in the domain. Based on this operator, we can calculate the energy norms of the extended Helmholtz-harmonic function. This leads to the required norms as well as the positive definite matrices defining these norms⁵.

With the discretized matrices constructed, the next step is to compute the top m left singular vectors of R_e for some selected $m \in \mathbb{N}$. This SVD problem turns out to be a generalized eigenvalue problem for these discrete matrices. For each e , denote the singular vectors by $\tilde{v}_{1,e}, \dots, \tilde{v}_{m,e} \in H_{00}^{1/2}(e)$. Their Helmholtz-harmonic extensions to the domain are denoted by $v_{1,e}, \dots, v_{m,e} \in \mathcal{H}(\Omega)$, obtained via the correspondance (3.8). The basis function space formed by the collection of all $v_{j,e}, 1 \leq j \leq m$ and $e \in \mathcal{E}_H$, together with the interpolation part $\{\psi_i\}_{x_i \in \mathcal{N}_H}$, are denoted by $V_{H,m}^{\text{off}}$. Note that here $\{\psi_i\}_{x_i \in \mathcal{N}_H}$ are the same as the basis functions in the MsFEM.

5.2.2. Online Stage. In the online stage, we solve u^h and u^b separately.

For the bubble part u^b , we solve the local Helmholtz problem in each element $T \in \mathcal{T}_H$, which leads to u_T^b defined in (3.2). Gluing them together leads to u^b .

⁵See also the implementation in Subsection 4.2 of [7] on how these matrices are constructed for elliptic problems.

The treatment for the Helmholtz-harmonic part is more delicate, depending on how to choose the trial and test spaces in the Galerkin method. We will outline four possible choices below.

The first two choices adhere strictly to our theoretical results. For each $e \in \mathcal{E}_H$ and ω_e , we construct the oversampling bubble part $u_{\omega_e}^b$ via solving a local helmholtz equation. Then, we get an edge function $R_e u_{\omega_e}^b$ for each edge. We add the Helmholtz-harmonic extension of these edge functions to the offline space of basis function $V_{H,m}^{\text{off}}$, leading to $V_{H,m}$ as defined in Subsection 3.4.4. The construction of this space requires the information of the right hand side f , so it is not offline; we call it online basis. The two choices for this case are

- Online basis + Ritz-Galerkin: use $S = V_{H,m} + \overline{V_{H,m}^{\text{off}}}$ and $S_{\text{test}} = S$ to solve (4.1).
- Online basis + Petrov-Galerkin: use $S = V_{H,m}$ and $S_{\text{test}} = \overline{V_{H,m}^{\text{off}}}$ to solve (4.1).

Our theoretical results imply that the approach of “online basis + Ritz-Galerkin” leads to a nearly exponential rate of convergence, which we will also demonstrate in our experiments. Nevertheless, using online basis requires us to update the stiffness matrix in the computation every time for a new right hand side. Practically, it is more appealing to use offline basis functions. This leads to the following two variants of our algorithm:

- Offline basis + Ritz-Galerkin: use $S = V_{H,m}^{\text{off}} + \overline{V_{H,m}^{\text{off}}}$ and $S_{\text{test}} = S$ to solve (4.1).
- Offline basis + Petrov-Galerkin: use $S = V_{H,m}^{\text{off}}$ and $S_{\text{test}} = \overline{V_{H,m}^{\text{off}}}$ to solve (4.1).

Since we ignore the oversampling bubble part, our theory only guarantees $O(H)$ error in the energy norm, and $O(H^2)$ error in the L^2 norm for such algorithms. Surprisingly, our numerical experiments will demonstrate that the offline basis approaches also lead to nearly exponential convergence. This observation extends our theoretical results considerably and yields a practical numerical algorithm that efficiently handles multiple right hand sides.

We note that all the above algorithms consider a uniform number of basis functions, namely m , for each edge $e \in \mathcal{E}_H$. It is also possible to make this number vary with edges, thus fully adaptive to the problem’s local properties. Consequently, this will lead to an adaptive algorithm where the truncated singular values serve as local error indicators. We do not pursue this in detail here and will leave this to our future work.

In the following, we will test our algorithms for different model problems. Our general set-up is to fix a reasonable coarse scale H and then study how the errors behave as m changes, for the four choices outlined above.

Remark 5.1. Our numerical experience implies that in the Ritz-Galerkin method, one does not need to add the conjugate space $\overline{V_{H,m}^{\text{off}}}$ or $\overline{V_{H,m}^{\text{off}}}$ into S while still obtaining an exponential rate of convergence. Thus, we will use $S = V_{H,m}$ or $V_{H,m}^{\text{off}}$ also in the Ritz-Galerkin method for our subsequent numerical experiments. Moreover, in the online basis approach, the space $V_{H,m}$ contains $R_e u_{\omega_e}^b$ for each e , which becomes zero when the right hand side in ω_e is zero. For the sake of numerical implementation, when $R_e u_{\omega_e}^b = 0$, we replace it by a quadratic function on e with zero boundary values; this guarantees the resulting stiffness matrix is invertible.

5.3. A High Wavenumber Example. We start with an example where the coefficients are constant and the wavenumber is high. More precisely, we set $A = V = \beta = 1$ and $f = 0$. The wavenumber $k = 2^7$. We take the exact solution to be

$$u(x_1, x_2) = \exp(-ik(0.6x_1 + 0.8x_2)).$$

Using this solution, we are able to specify the Robin boundary condition on $\partial\Omega$. Note that this is an inhomogeneous boundary condition, so it is beyond our previous theoretical discussion. In this case, the inhomogeneous data are incorporated to the equation of the bubble part u^b , while the treatment for the Helmholtz-harmonic part remains the same as that in the homogeneous case.

We set the fine mesh $h = 2^{-10}$, coarse mesh $H = 2^{-5}$. We vary the number of edge basis functions in each $e \in \mathcal{E}_H$, choosing $m = 1, 2, \dots, 7$ and implementing the four algorithms outlined in Subsection 5.2.2. The results are shown in Figure 5.2. We

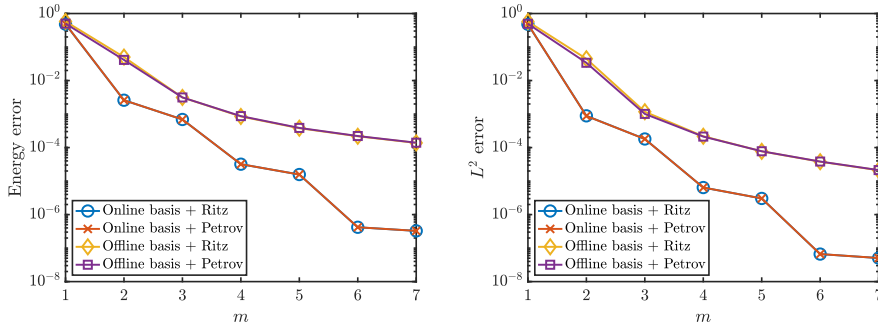


FIG. 5.2. Numerical results for the high wavenumber example. Left: e_H versus m ; right: e_{L^2} versus m .

observe that the online basis approaches achieve nearly exponential decaying errors with respect to m . The difference between the Ritz-Galerkin and Petrov-Galerkin approaches is almost negligible. If the oversampling bubble part is not computed and the offline basis approaches are used, we still have a nearly exponential decay of errors, though the errors are worse compared to their online basis counterparts.

5.4. A Varying Wavelength Example. Here we consider an example with a varying V . We choose $A = 1$, $k = 2^7$, $\beta = 1$. The function V takes values 1 or 2, where $V = 2$ in some periodically spaced blocks which form the domain

$$(5.2) \quad D = \bigcup_{j \in \{2, 3, \dots, 8\}^2} 0.1(j + (-0.25, 0.25)^2).$$

Let $y = (0.5, 0.5)$ and $\text{dist}(x, y)^2 = (x_1 - 0.5)^2 + (x_2 - 0.5)^2$. The right hand side is set to be

$$f(x_1, x_2) = \begin{cases} \exp(-\frac{1}{1 - 400 \times \text{dist}(x, y)^2}), & \text{dist}(x, y)^2 < \frac{1}{400} \\ 0, & \text{otherwise.} \end{cases}$$

We impose the homogeneous Robin boundary condition on $\partial\Omega$. We take the fine mesh $h = 2^{-10}$ and the coarse mesh $H = 2^{-5}$. We take $m = 1, 2, \dots, 7$ and the numerical results are shown in Figure 5.3. Again we observe a nearly exponential rate of convergence.

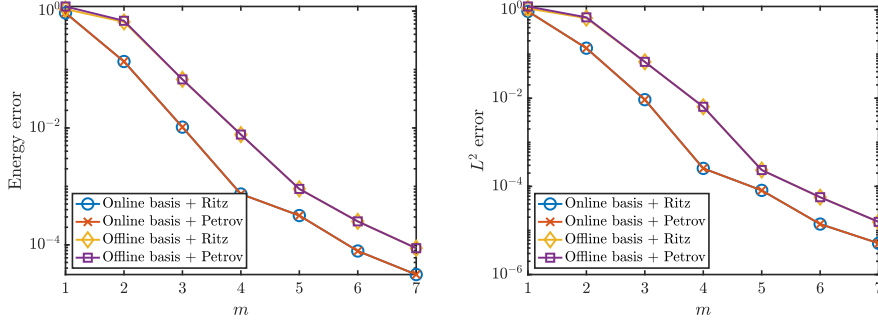


FIG. 5.3. Numerical results for the varying wavelength example. Left: $e_{\mathcal{H}}$ versus m ; right: e_{L^2} versus m .

5.5. A High Contrast Example. In the third example, we consider an $A(x)$ with high contrast channels. Let

$$X := \{(x_1, x_2) \in [0, 1]^2, x_1, x_2 \in \{0.2, 0.3, \dots, 0.8\}\} \subset [0, 1]^2,$$

and the coefficient is defined as

$$A(x) = \begin{cases} 1, & \text{if } \text{dist}(x, X) \geq 0.025 \\ M, & \text{else.} \end{cases}$$

Here, M is a parameter controlling the contrast. We choose $M = 2^{12}$ and visualize $\log_{10} A(x)$ in the left plot of Figure 5.4.

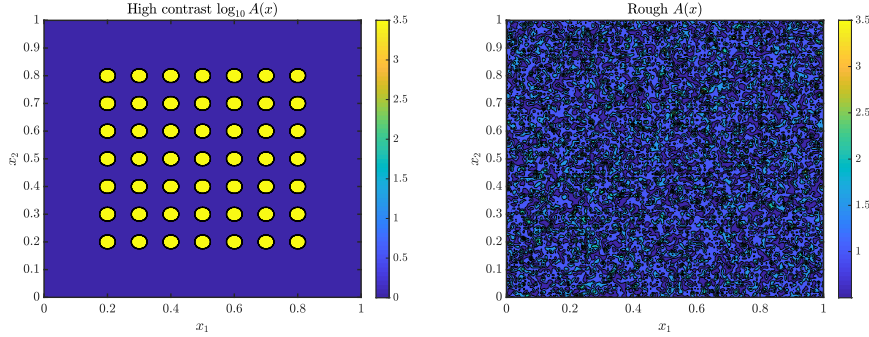


FIG. 5.4. Left: the contour of $\log_{10} A$ for the high contrast example; right: the contour of A for the rough media example.

We take $\beta = 1, V = 1, k = 2^5$. The right hand side is

$$f(x_1, x_2) = \begin{cases} 10000 \exp\left(-\frac{1}{1 - 400 \times \text{dist}(x, z)^2}\right), & \text{dist}(x, z)^2 < \frac{1}{400} \\ 0, & \text{otherwise,} \end{cases}$$

where $z = (0.125, 0.5)$ and $\text{dist}(x, z)^2 = (x_1 - 0.125)^2 + (x_2 - 0.5)^2$. We impose the homogeneous Robin boundary condition on $\partial\Omega$. We take the fine mesh $h = 2^{-10}$

and the coarse mesh $H = 2^{-5}$. As before we take $m = 1, 2, \dots, 7$ and the numerical results are shown in Figure 5.3. A nearly exponential rate of convergence is observed consistently, and all the four methods behave similarly.

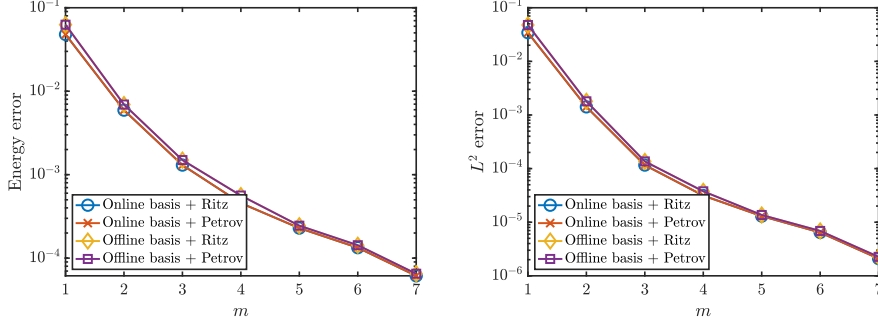


FIG. 5.5. Numerical results for the high contrast example. Left: $e_{\mathcal{H}}$ versus m ; right: e_{L^2} versus m .

5.6. A Mixed Boundary and Rough Field Example. In the last example, we consider a mixed boundary problem. We impose the homogeneous Dirichlet boundary condition on $(x_1, 0), x_1 \in [0, 1]$, the homogeneous Neumann boundary condition on $(x_1, 1), x_1 \in [0, 1]$, and the homogeneous Robin boundary condition on the other two parts of $\partial\Omega$. We choose $A(x)$ to be a realization of some random field; more precisely,

$$(5.3) \quad A(x) = |\xi(x)| + 0.5,$$

where the field $\xi(x)$ satisfies

$$\xi(x) = a_{11}\xi_{i,j} + a_{21}\xi_{i+1,j} + a_{12}\xi_{i,j+1} + a_{22}\xi_{i+1,j+1}, \text{ if } x \in \left[\frac{i}{2^7}, \frac{i+1}{2^7}\right) \times \left[\frac{j}{2^7}, \frac{j+1}{2^7}\right).$$

Here, $\{\xi_{i,j}, 0 \leq i, j \leq 2^7\}$ are i.i.d. unit Gaussian random variables. In addition, $a_{11} = (i+1-2^7x_1)(j+1-2^7x_2)$, $a_{21} = (2^7x_1-i)(j+1-2^7x_2)$, $a_{12} = (i+1-2^7x_1)(2^7x_2-j)$, $a_{22} = (2^7x_1-i)(2^7x_2-j)$ are interpolating coefficients to make $\xi(x)$ piecewise linear. A sample from this field is displayed in the right plot of Figure 5.4.

Moreover, we also take $V(x)$ and $\beta(x)$ as independent samples drawn from this random field. We choose the wavenumber $k = 2^5$. The right hand side is

$$f(x_1, x_2) = \begin{cases} 10000 \exp\left(-\frac{1}{1 - 400 \times \text{dist}(x, z)^2}\right), & \text{dist}(x, z)^2 < \frac{1}{400} \\ 0, & \text{otherwise,} \end{cases}$$

where $z = (0.125, 0.5)$ and $\text{dist}(x, z)^2 = (x_1 - 0.125)^2 + (x_2 - 0.5)^2$. The fine mesh $h = 2^{-10}$ and the coarse mesh $H = 2^{-5}$. Again we take $m = 1, 2, \dots, 7$ and present the numerical results in Figure 5.6. A nearly exponential rate of convergence is still observed for this challenging example. The differences between the Ritz-Galerkin method and Petrov-Galerkin method, as well as between the online basis and offline basis approaches, are very mild. It is worth noting that this example is constructed artificially, mixing different kinds of boundary conditions and rough coefficients, without taking into account the analytical properties of this combination. Thus, the

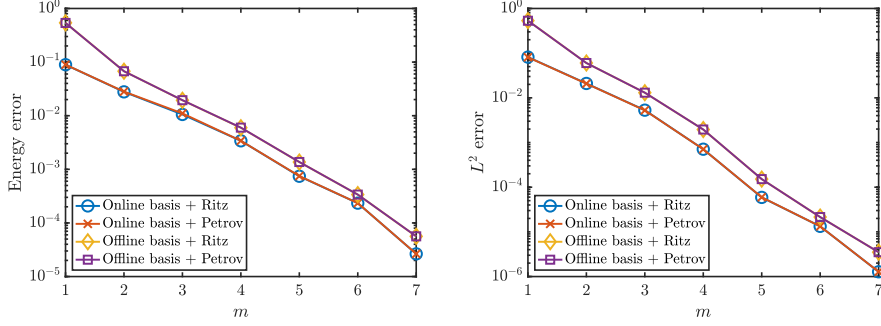


FIG. 5.6. Numerical results for the mixed boundary and rough field example. Left: $e_{\mathcal{H}}$ versus m ; right: e_{L^2} versus m .

numerical results for this example demonstrate the effectiveness of our multiscale methods in a more general setting.

5.7. Summary. We make a summary of what we have observed in these numerical examples. All of the four choices of algorithms lead to a nearly exponential rate of convergence with respect to m . Online basis approaches are more accurate than offline basis approaches; however, the latter will be more computationally efficient since there is no need to update the stiffness matrix for different right hand sides. As the difference between the online and offline approaches is not very significant, it is preferable to use the offline approaches in practice, especially for the setting of multiple $f(x)$.

Moreover, it is observed that the difference between the Ritz-Galerkin and the Petrov-Galerkin approaches is very mild. As mentioned in Remark 4.10, the Petrov-Galerkin approach is computationally more efficient since one does not need to compute the additional effective equation for u^h . Therefore, we recommend using the Petrov-Galerkin approach in practice, combined with the offline basis setting to handle multiple right hand sides.

6. Proofs. This section presents the theoretical proofs in this paper. Some proofs are similar to those in the elliptic case. We will refer these proofs to the corresponding proofs in the elliptic case [7], while we will make relevant remarks on possible changes and modifications.

6.1. Proof of Proposition 2.1. In this subsection, we provide the proof of the qualitative version of C^α estimate. It is a direct application of related results for elliptic equations. We need to be careful to apply these results so that the constant is independent of k .

Proof. We note that the Helmholtz PDE (1.1) is equivalent to

$$(6.1) \quad \begin{cases} -\nabla \cdot (A \nabla u) = f + k^2 V^2 u, & \text{in } \Omega \\ u = 0, & \text{on } \Gamma_D \\ A \nabla u \cdot \nu = T_k u, & \text{on } \Gamma_N \cup \Gamma_R. \end{cases}$$

Since $f \in L^2(\Omega)$, we know by the a priori estimate of the Helmholtz equation that $u \in H^1(\Omega)$. Therefore we can regard (6.1) as an elliptic PDE with $k^2 V^2 u$ known as a part of the right hand side. This PDE has its right hand side in $L^2(\Omega)$ and has

its solution coinciding with u . We can invoke the result in Remark 6.5 of [19], which concludes that u lies in some Hölder space $C^\alpha(\Omega)$ such that

$$\|u\|_{C^\alpha(\Omega)} \leq C(\|f\|_{L^2(\Omega)} + k^2\|u\|_{L^2(\Omega)}),$$

for some Hölder exponent $\alpha \in (0, 1)$ and C . \square

6.2. Proof of Proposition 3.6. The proof relies on the fact that any function v on e belonging to $H^{1/2}(e) \cap C^\alpha(e)$ and vanishing at ∂e will be in the space $H_{00}^{1/2}(e)$; see Proposition 2.1 in [7] for detailed arguments of this fact. Then, $R_e \tilde{u}^h \in H^{1/2}(e) \cap C^\alpha(e)$ and vanishes at ∂e , so it belongs to $H_{00}^{1/2}(e)$.

6.3. Proof of Theorem 3.8. We decompose the energy norm into the contribution from each element $T \in \mathcal{T}_H$:

$$\|u^h - I_H u^h - \sum_{e \in \mathcal{E}_H} v_e\|_{\mathcal{H}(\Omega)}^2 = \sum_{T \in \mathcal{T}_H} \|u^h - I_H u^h - \sum_{e \sim T} v_e\|_{\mathcal{H}(T)}^2,$$

where we have used the fact that $v_e = 0$ in T if e and T are not neighbors.

Let us fix an element T . For each $e \sim T$, the trace of the function $u^h - I_H u^h - \sum_{e \in T} v_e$ on e is $\tilde{u}^h - I_H \tilde{u}^h - \tilde{v}_e \in H_{00}^{1/2}(e)$. We can extend this trace to $\partial T \setminus e$ by 0 to get an $H^{1/2}(\partial T)$ boundary data. Then, this boundary data can be used to define a Helmholtz-harmonic function in T , via the correspondance (3.8). Using the triangle inequality and the Cauchy-Schwarz inequality, we get

$$\|u^h - I_H u^h - \sum_{e \sim T} v_e\|_{\mathcal{H}(T)}^2 \leq C_{\text{mesh}} \sum_{e \sim T} \|P_e(\tilde{u}^h - I_H \tilde{u}^h) - \tilde{v}_e\|_{\mathcal{H}_T^{1/2}(e)}^2,$$

where the $\mathcal{H}_T^{1/2}(e)$ norm of a function $\tilde{\psi} \in H_{00}^{1/2}(e)$ is defined as

$$(6.2) \quad \|\tilde{\psi}\|_{\mathcal{H}_T^{1/2}(e)}^2 := \int_T A|\nabla \psi|^2 + k^2|V\psi|^2.$$

The constant C_{mesh} depends on the mesh type only; for example $C_{\text{mesh}} = 4$ for the quadrilateral mesh and $C_{\text{mesh}} = 3$ for the triangular mesh. Then, we sum the above inequality over all $T \in \mathcal{T}_H$, which yields

$$\begin{aligned} \|u^h - I_H u^h - \sum_{e \in \mathcal{E}_H} v_e\|_{\mathcal{H}(\Omega)}^2 &\leq C_{\text{mesh}} \sum_{T \in \mathcal{T}_H} \sum_{e \sim T} \|P_e(\tilde{u}^h - I_H \tilde{u}^h) - \tilde{v}_e\|_{\mathcal{H}_T^{1/2}(e)}^2 \\ (6.3) \quad &= C_{\text{mesh}} \sum_{e \in \mathcal{E}_H} \|P_e(\tilde{u}^h - I_H \tilde{u}^h) - \tilde{v}_e\|_{\mathcal{H}^{1/2}(e)}^2 \\ &\leq C_{\text{mesh}} \sum_{e \in \mathcal{E}_H} \epsilon_e^2. \end{aligned}$$

The proof is completed.

6.4. Proof of Theorem 3.10. This is the key theorem underlying the exponential convergence for approximating u^h . To prove it, we need to analyze the spectrum of the operator R_e for each edge e . The treatments for interior edges and edges connected to the boundary are slightly different, due to the different boundary conditions involved. We will explain the proof for interior edges in detail and comment on the changes needed to be made for edges connected to the boundary.

Since this theorem is stated for all edges, we start by discussing some geometric relations that hold uniformly for every interior edge.

6.4.1. Geometric Relation. Suppose e is an interior edge, so that e lies strictly in the interior domain of ω_e ; see Figure 3.2. We describe some geometric relation⁶ between e and ω_e that will be needed in our analysis. Figure 6.1 illustrates our ideas for a uniform quadrilateral mesh. For each interior edge e , there exists two concentric rectangles $\omega \subset \omega^* \subset \omega_e$ with center being the midpoint m_e of e , such that $e \subset \omega \subset \omega^* \subset \omega_e$; the center m_e is the center of gravity of ω and ω^* . We require $\omega^* \cap \partial\Omega = \emptyset$. Moreover, one side of ω and ω^* should be parallel to e . We introduce three parameters l_1, l_2, l_3 to specify and describe the geometry:

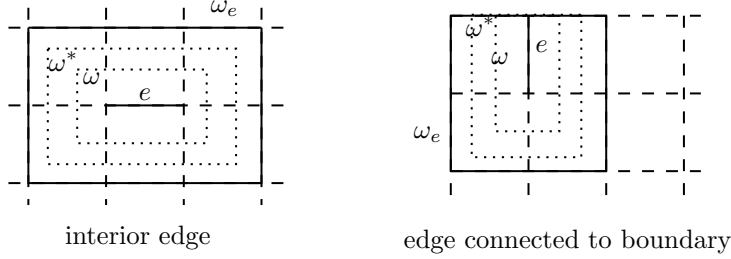


FIG. 6.1. Geometric relation $e \subset \omega \subset \omega^* \subset \omega_e$

1. With respect to the center m_e , the two rectangles ω and ω^* are scaling equivalent, such that there exists $l_1 > 1$, $\omega^* - m_e = l_1 \cdot (\omega - m_e)$. Here we use the notation that $t \cdot X := \{tx : x \in X\}$ for a set X and a scalar t . For our choice of ω_e , the parameter l_1 can be selected to only depend on c_0 and c_1 in Subsection 3.1.1.
2. The ratio of ω 's larger side length over the smaller side length is bounded by a uniform constant $l_2 > 1$ that depends on c_0 and c_1 only.
3. There is a constant $l_3 > 1$ depending on c_0 and c_1 only such that $l_3 \cdot e \subset \omega$.

We note that l_1, l_2, l_3 are universal constants for all interior edges. All three parameters depend on c_0, c_1 only. We introduce these parameters in order to get a uniform treatment for every interior edge. Indeed, several constants in our estimates depend on l_1, l_2, l_3 , but not on k and H , uniformly for all interior edges.

6.4.2. Main Idea of the Proof. In the following, we explain the main ideas of our proof. Recall the target is to show the left singular values of R_e decays nearly exponentially fast. Similar to the rationale behind (3.17), it suffices to show there exists an $m - 1$ dimensional space $W_{m,e} \subset H_{00}^{1/2}(e)$ such that

$$(6.4) \quad \min_{\tilde{v}_e \in W_{m,e}} \|R_e v - \tilde{v}_e\|_{\mathcal{H}^{1/2}(e)} \leq C_\epsilon \exp\left(-m^{(\frac{1}{d+1}-\epsilon)}\right) \|v\|_{\mathcal{H}(\omega_e)},$$

for any $v \in U(\omega_e)$. We also use $U(\omega')$ to denote the function space in ω' defined via (3.15) with ω_e replaced by any ω' . Our proof contains two main steps, summarized in the following two lemmas.

LEMMA 6.1. *For any $v \in U(\omega^*)$, there exists an $m - 1$ dimensional space $\Phi_{m,e} \subset U(\omega)$ such that*

$$(6.5) \quad \min_{\chi \in \Phi_{m,e}} \|v - \chi\|_{\mathcal{H}(\omega)} \leq C_\epsilon \exp\left(-m^{(\frac{1}{d+1}-\epsilon)}\right) \|v\|_{\mathcal{H}(\omega^*)},$$

for some C_ϵ independent of k and H .

⁶It is similar to that in Subsection 3.3.1 of [7].

LEMMA 6.2. *For any $v \in H^1(\omega)$ and $\nabla \cdot (A\nabla v) \in L^2(\omega)$, it holds that*

$$(6.6) \quad \|R_e v\|_{\mathcal{H}^{1/2}(\omega_e)} \leq C \left(\|v\|_{\mathcal{H}(\omega)} + H \|\nabla \cdot (A\nabla v) + k^2 V^2 v\|_{L^2(\omega)} \right),$$

for some C independent of k and H .

We will defer the proofs of the two lemmas to Subsections 6.4.3 and 6.4.6, and describe how to prove Theorem 3.10 using them here.

Proof of Theorem 3.10. From the above discussion, it remains to show (6.4). For $v \in \mathcal{H}(\omega_e)$, we have $v \in \mathcal{H}(\omega^*)$ and $\|v\|_{\mathcal{H}(\omega^*)} \leq \|v\|_{\mathcal{H}(\omega_e)}$. By Lemma 6.1, we get

$$\min_{\chi \in \Phi_{m,e}} \|v - \chi\|_{\mathcal{H}(\omega)} \leq C_\epsilon \exp\left(-m^{(\frac{1}{d+1}-\epsilon)}\right) \|v\|_{\mathcal{H}(\omega_e)}.$$

Now since $v - \chi$ satisfies the condition in Lemma 6.2 and v and χ both vanish under the operator $v \rightarrow \nabla \cdot (A\nabla v) + k^2 V^2 v$, we obtain

$$\min_{\chi \in \Phi_{m,e}} \|R_e v - R_e \chi\|_{\mathcal{H}^{1/2}(\omega_e)} \leq C C_\epsilon \exp\left(-m^{(\frac{1}{d+1}-\epsilon)}\right) \|v\|_{\mathcal{H}(\omega_e)}.$$

Thus, taking $W_{m,e} = R_e \Phi_{m,e}$ completes the proof. \square

6.4.3. Proof of Lemma 6.1. The proof of this lemma is inspired by Theorem 3.3 in [1], which states a similar result but for elliptic equations only. We generalize it here for the Helmholtz equation.

First, by our geometric construction, $\omega^* - m_e = l_1 \cdot (\omega - m_e)$. We denote a sequence of domains $\omega = \omega_0 \subset \omega_1 \subset \dots \subset \omega_{N-1} \subset \omega_N = \omega^*$ such that they are concentric and that $\omega_j - m_e = (1+t)(\omega_{j-1} - m_e)$ for $j = 1, 2, \dots, N$. Here $t = l_1^{1/N} - 1$. Then, there are two important lemmas, whose proofs are presented in Subsections 6.4.4 and 6.4.5.

LEMMA 6.3. *For each $0 \leq j \leq N$ and any $n \in \mathbb{N}$, there is an n -dimensional space $W_n(\omega_j) \subset U(\omega_j)$, such that for all $v \in U(\omega_j)$, it holds that*

$$(6.7) \quad \inf_{w \in W_n(\omega_j)} \|v - w\|_{L^2(\omega_j)} \leq C H n^{-1/d} \|v\|_{\mathcal{H}(\omega_j)},$$

where C is a generic constant independent of k, H, t and n .

LEMMA 6.4. *For each $1 \leq j \leq N$ and every $v \in U(\omega_j)$, it holds that*

$$(6.8) \quad \|v\|_{\mathcal{H}(\omega_{j-1})} \leq (C/tH) \|v\|_{L^2(\omega_j)},$$

where C is a generic constant independent of k, H and t .

With the two lemmas, we are ready to prove Lemma 6.1.

Proof of Lemma 6.1. Choose $n = \lfloor m/N \rfloor$. The proof relies on an iteration argument. We start from $j = N$. By (6.7) and (6.8), we get an n dimensional space $W_n(\omega_N) \subset U(\omega_N)$ and a function $w_N \in W_n(\omega_N)$ such that

$$\|v - w_N\|_{\mathcal{H}(\omega_{N-1})} \leq (C/tH) \|v - w_N\|_{L^2(\omega_N)} \leq C t^{-1} n^{-1/d} \|v\|_{\mathcal{H}(\omega_N)},$$

where we have used the fact that the infimum in (6.7) is attained since it is a finite dimensional optimization problem. Here by abuse of notation the value of the constant C varies in different places. It is a generic constant independent of k, H, t and n .

Now, we iterate the above process. The function $v - w_N \in U(\omega_{N-1})$, so again by (6.7) and (6.8), we get an n dimensional space $W_n(\omega_{N-1}) \subset U(\omega_{N-1})$ and a function $w_{N-1} \in W_n(\omega_{N-1})$ such that

$$\|v - w_N - w_{N-1}\|_{\mathcal{H}(\omega_{N-2})} \leq Ct^{-1}n^{-1/d}\|v - w_N\|_{\mathcal{H}(\omega_{N-1})} \leq (Ct^{-1}n^{-1/d})^2\|v\|_{\mathcal{H}(\omega_N)}.$$

Repeating the above procedure, we get

$$\|v - \sum_{j=1}^N w_j\|_{\mathcal{H}(\omega)} \leq (Ct^{-1}n^{-1/d})^N\|v\|_{\mathcal{H}(\omega^*)},$$

where each $w_j \in U(\omega_j) \subset U(\omega_0) = U(\omega)$. Therefore, there exists an $nN \leq m$ dimensional space $\Phi_{m,e} \subset U(\omega)$ such that

$$\inf_{w \in \Phi_{m,e}} \|v - w\|_{\mathcal{H}(\omega)} \leq (Ct^{-1}n^{-1/d})^N\|v\|_{\mathcal{H}(\omega^*)}.$$

Choose $N = \left\lfloor m^{\frac{q}{q+1}} \right\rfloor$, then we obtain

$$(6.9) \quad (Ct^{-1}n^{-1/d})^N \leq \left(Ct^{-1}\left(\frac{m}{N}\right)^{-1/d}\right)^N = \exp\left(N\left(\frac{1}{d}\log\left(\frac{N}{m}\right) + \log C - \log t\right)\right).$$

Using $N \leq m^{\frac{q}{q+1}}$ and $t = l_1^{1/N} - 1 = \exp(\frac{1}{N}\log l_1) - 1 \geq \frac{1}{N}\log l_1 \geq m^{-\frac{q}{q+1}}\log l_1$, we can bound the right hand side of (6.9) as

$$(6.10) \quad \begin{aligned} (Ct^{-1}n^{-1/d})^N &\leq \exp\left(-m^{\frac{q}{q+1}}\left(\left(\frac{1}{d} - q\right)\frac{1}{q+1}\log m - \log C + \log \log l_1\right)\right) \\ &\leq C_q \exp\left(-m^{\frac{q}{q+1}}\right), \end{aligned}$$

for some constant C_q that depends on q, d, C, l_1 , if $q < 1/d$. This condition implies the exponent $\frac{q}{q+1} < \frac{1}{d+1}$. Denote $\frac{q}{q+1} = \frac{1}{d+1} - \epsilon$ for some $\epsilon > 0$. We can also write in terms of ϵ as

$$(Ct^{-1}n^{-1/d})^N \leq C_\epsilon \exp\left(-m^{\frac{1}{d+1}-\epsilon}\right),$$

which completes the proof. \square

6.4.4. Proof of Lemma 6.3. First, using the spectrum of the Laplacian operator with Neumann's boundary condition, there exists an n dimensional space $S_n \subset H^1(\omega_j)$ such that for any $v \in H^1(\omega_j)$,

$$(6.11) \quad \inf_{w \in S_n} \|v - w\|_{L^2(\omega_j)} \leq CHn^{-1/d}\|v\|_{H^1(\omega_j)} \leq CHn^{-1/d}\|v\|_{\mathcal{H}(\omega_j)},$$

where C is a generic constant independent of k, H, t and n . Equivalently, this implies the identity embedding operator $Q : (\mathcal{H}(\omega_j), \|\cdot\|_{\mathcal{H}(\omega_j)}) \rightarrow (L^2(\omega_j), \|\cdot\|_{L^2(\omega_j)})$ such that $Qv = v$ is compact and the its n -th largest left singular value $\mu_n \leq CHn^{-1/d}$.

Now, since $U(\omega_j)$ is a closed subspace of $(\mathcal{H}(\omega_j), \|\cdot\|_{\mathcal{H}(\omega_j)})$, we can view Q as an operator from $(U(\omega_j), \|\cdot\|_{\mathcal{H}(\omega_j)})$ to $(L^2(\omega_j), \|\cdot\|_{L^2(\omega_j)})$. Denote its singular values in a non-increasing order by $\{\mu'_n\}$. Using the max-min theorem for singular values, we obtain

$$\begin{aligned} \mu'_n &= \max_{S_n \subset U(\omega_j), \dim(S_n)=n} \min_{v \in S_n, \|v\|_{\mathcal{H}(\omega_j)}=1} \|Qv\|_{L^2(\omega_j)} \\ &\leq \max_{S_n \subset \mathcal{H}(\omega_j), \dim(S_n)=n} \min_{v \in S_n, \|v\|_{\mathcal{H}(\omega_j)}=1} \|Qv\|_{L^2(\omega_j)} = \mu_n. \end{aligned}$$

Thus, $\mu'_n \leq CHn^{-1/d}$. Therefore, there is an n -dimensional space $W_n(\omega_j) \subset U(\omega_j)$, such that for all $v \in U(\omega_j)$, it holds that

$$\inf_{w \in S_n} \|v - w\|_{L^2(\omega_j)} \leq CHn^{-1/d} \|v\|_{H^1(\omega_j)} \leq CHn^{-1/d} \|v\|_{\mathcal{H}(\omega_j)}.$$

The proof is completed.

6.4.5. Proof of Lemma 6.4. We introduce a cutoff function $\eta \in C^1(\omega_j)$ such that $0 \leq \eta \leq 1$, and $\eta = 1$ in ω_{j-1} , as well as $|\nabla \eta(x)| \leq C/(tH)$ for some constant C independent of k, H and t .

For any $v \in U(\omega_j)$, we use the test function $\eta^2 v$ and the weak form to get

$$(6.12) \quad (A \nabla v, \nabla(\eta^2 v))_{\omega_j} - k^2 (Vv, V\eta^2 v)_{\omega_j} = 0,$$

where we have used the definition of $U(\omega_j)$ (see the beginning of Subsection 6.4.2), and the property of our construction that $\partial\omega_j \cap (\Gamma_N \cup \Gamma_R) = \emptyset$.

Using the relation $\|A^{1/2} \eta \nabla v\|_{L^2(\omega_j)}^2 = (A \nabla v, \eta^2 \nabla v)_{\omega_j}$ and the above formula, we obtain

$$(6.13) \quad \begin{aligned} \|A^{1/2} \eta \nabla v\|_{L^2(\omega_j)}^2 &= -2(A^{1/2} \eta \nabla v, A^{1/2} v \nabla \eta)_{\omega_j} + k^2 (Vv, V\eta^2 v)_{\omega_j}, \\ &\leq \frac{1}{2} \|A^{1/2} \eta \nabla v\|_{L^2(\omega_j)}^2 + 2 \|A^{1/2} v \nabla \eta\|_{L^2(\omega_j)}^2 + k^2 V_{\max}^2 \|v\|_{L^2(\omega_j)}^2, \end{aligned}$$

which leads to $\|A^{1/2} \eta \nabla v\|_{L^2(\omega_j)}^2 \leq 4 \|A^{1/2} v \nabla \eta\|_{L^2(\omega_j)}^2 + 2k^2 V_{\max}^2 \|v\|_{L^2(\omega_j)}^2$. Therefore, using the fact that $\eta = 1$ in ω_{j-1} , we have

$$(6.14) \quad \begin{aligned} \|v\|_{\mathcal{H}(\omega_{j-1})}^2 &\leq \|A^{1/2} \eta \nabla v\|_{L^2(\omega_j)}^2 + k^2 V_{\max}^2 \|v\|_{L^2(\omega_j)}^2 \\ &\leq 4 \|A^{1/2} v \nabla \eta\|_{L^2(\omega_j)}^2 + 3k^2 V_{\max}^2 \|v\|_{L^2(\omega_j)}^2 \\ &\leq \left(\frac{4C^2}{(tH)^2} + 3k^2 V_{\max}^2 \right) \|v\|_{L^2(\omega_j)}^2 \\ &\leq \frac{C'^2}{(tH)^2} \|v\|_{L^2(\omega_j)}^2, \end{aligned}$$

for some C' independent of k, H and t , where we have used Assumption 1 such that $kV_{\max}H \leq C''$ for $C'' = A_{\min}^{1/2}/(\sqrt{2}C_P)$. This completes the proof.

6.4.6. Proof of Lemma 6.2. We use Lemma 3.9 of [7], which implies that

$$(6.15) \quad \|R_e v\|_{\mathcal{H}^{1/2}(e)} \leq C \left(\|A^{1/2} \nabla v\|_{L^2(\omega)} + H \|\nabla \cdot (A \nabla v)\|_{L^2(\omega)} \right),$$

for some C independent of k, H . By a triangular inequality, we have

$$\begin{aligned} H \|\nabla \cdot (A \nabla v)\|_{L^2(\omega)} &\leq H \|k^2 V^2 v\|_{L^2(\omega)} + H \|\nabla \cdot (A \nabla v) + k^2 V^2 v\|_{L^2(\omega)} \\ &\leq C' \|kVv\|_{L^2(\omega)} + H \|\nabla \cdot (A \nabla v) + k^2 V^2 v\|_{L^2(\omega)}, \end{aligned}$$

where we have used Assumption 1 such that $kV_{\max}H \leq C'$ for $C' = A_{\min}^{1/2}/(\sqrt{2}C_P)$. Now, using the definition of the $\mathcal{H}(\omega)$ norm, we have

$$\|A^{1/2} \nabla v\|_{L^2(\omega)} + C' \|kVv\|_{L^2(\omega)} \leq C'' \|v\|_{\mathcal{H}(\omega)},$$

for some generic constant C'' that does not depend on anything else. Combining the above inequalities concludes the proof.

6.4.7. For Edges Connected to the Boundary. The above proofs are for interior edges. For edges connected to the boundary, we need a different geometric relation, as depicted in the right of Figure 6.1. The quantitative characterization of this geometric relation is the same as that in Subsection 3.3.2 of [7], which introduces three other parameters l_4, l_5, l_6 to describe the geometry associated with edges, similar to l_1, l_2, l_3 for interior edges.

The main idea of the proof for this case is the same as that for the interior edges. We need to prove Lemmas 6.1 and 6.2 for edges connected to the boundary. The proof of Lemma 6.2 remains the same since its statement holds for all edges. To prove Lemma 6.1, we again use the same strategy in Subsection 6.4.3, by establishing Lemmas 6.3 and 6.4 and then using an iteration argument. The iteration argument and the proof for Lemma 6.3 remain unchanged. For Lemma 6.4, the only slight change is (6.12), which becomes

$$(6.16) \quad (A\nabla v, \nabla(\eta^2 v))_{\omega_j} - k^2(Vv, V\eta^2 v)_{\omega_j} = (T_k v, \eta^2 v)_{\partial\omega_j \cap (\Gamma_N \cup \Gamma_R)},$$

due to the boundary conditions involved. However, since $\Re(T_k v, \eta^2 v)_{\partial\omega_j \cap (\Gamma_N \cup \Gamma_R)} \leq 0$, the conclusion of Lemma 6.4 still holds.

Therefore, the result also holds for edges connected to the boundary.

6.5. Proof of Proposition 3.11. First we have the bound on the oversampling bubble part in (3.21):

$$(6.17) \quad \|u_{\omega_e}^b\|_{\mathcal{H}(\omega_e)} \leq \frac{3C'_P}{A_{\min}^{1/2}} H \|f\|_{L^2(\omega_e)}.$$

Applying Lemma 6.2 and the definition of $u_{\omega_e}^b$ leads to

$$(6.18) \quad \begin{aligned} \|R_e u_{\omega_e}^b\|_{\mathcal{H}^{1/2}(e)} &\leq C (\|u_{\omega_e}^b\|_{\mathcal{H}(\omega)} + H \|\nabla \cdot (A\nabla u_{\omega_e}^b) + k^2 V^2 u_{\omega_e}^b\|_{L^2(\omega)}) \\ &\leq C' H \|f\|_{L^2(\omega_e)}, \end{aligned}$$

where C' is a constant independent of k and H .

7. Concluding Remarks. In this paper, we have developed a multiscale framework for solving the Helmholtz equation in heterogeneous media and high frequency regimes. The coarse-fine scale decomposition of the solution space is motivated by the MsFEM. In our algorithm, the coarse scale Helmholtz-harmonic part and the fine scale bubble part are computed separately. Their own structures are carefully explored, such as the low complexity of the coarse part and the locality of the fine part. A nearly exponential rate of convergence is proved rigorously and is confirmed numerically for a wide range of the Helmholtz equations with rough coefficients, high contrast, and mixed boundary conditions.

Perhaps surprisingly, our framework implies that designing an accurate multiscale method for the Helmholtz equation is not much more different from that for the elliptic equation. Many techniques in the elliptic case can be successfully adapted once the mesh size satisfies $H = O(1/k)$, a condition that does not suffer from the pollution effect. This work also demonstrates the broad applicability of our exponentially convergent multiscale framework proposed originally in [7].

Most discussions in this paper are concerned with dimension $d = 2$. As noted in Section 5.3 of [7], generalization to $d \geq 3$ requires a new localization strategy for the Helmholtz-harmonic part. Nodal interpolation is not enough since different

elements can interact via low dimensional cells other than nodes. One needs to design approximation spaces for all cells with co-dimension $1, 2, \dots, d$ that constitute the mesh.

In our future work, we would like to extend this methodology systematically to high dimensions and to other equations such as the Schrodinger equation, where the potential function could introduce indefiniteness into the system. Moreover, developing a better theoretical understanding of the behavior of the multiscale framework with respect to high contrast in the media is also an exciting direction for further exploration.

REFERENCES

- [1] I. BABUŠKA AND R. LIPTON, *Optimal local approximation spaces for generalized finite element methods with application to multiscale problems*, Multiscale Modeling & Simulation, 9 (2011), pp. 373–406.
- [2] I. BABUŠKA AND J. OSBORN, *Can a finite element method perform arbitrarily badly?*, Mathematics of Computation, 69 (2000), pp. 443–462.
- [3] I. M. BABUSKA AND S. A. SAUTER, *Is the pollution effect of the fem avoidable for the Helmholtz equation considering high wave numbers?*, SIAM Journal on numerical analysis, 34 (1997), pp. 2392–2423.
- [4] T. BETCKE, S. N. CHANDLER-WILDE, I. G. GRAHAM, S. LANGDON, AND M. LINDNER, *Condition number estimates for combined potential integral operators in acoustics and their boundary element discretisation*, Numerical Methods for Partial Differential Equations, 27 (2011), pp. 31–69.
- [5] D. L. BROWN, D. GALLISTL, AND D. PETERSEIM, *Multiscale Petrov-Galerkin method for high-frequency heterogeneous Helmholtz equations*, in Meshfree methods for partial differential equations VIII, Springer, 2017, pp. 85–115.
- [6] Y. CHEN AND T. Y. HOU, *Multiscale elliptic PDEs upscaling and function approximation via subsampled data*, arXiv preprint arXiv:2010.04199, (2020).
- [7] Y. CHEN, T. Y. HOU, AND Y. WANG, *Exponential convergence for multiscale linear elliptic PDEs via adaptive edge basis functions*, to appear in Multiscale Modeling & Simulation, arXiv preprint arXiv:2007.07418, (2020).
- [8] E. T. CHUNG, Y. EFENDIEV, AND W. T. LEUNG, *Constraint energy minimizing generalized multiscale finite element method*, Computer Methods in Applied Mechanics and Engineering, 339 (2018), pp. 298–319.
- [9] Y. EFENDIEV, J. GALVIS, AND T. Y. HOU, *Generalized multiscale finite element methods (GMs-FEM)*, Journal of Computational Physics, 251 (2013), pp. 116 – 135.
- [10] B. ENGQUIST AND L. YING, *Sweeping preconditioner for the Helmholtz equation: hierarchical matrix representation*, Communications on pure and applied mathematics, 64 (2011), pp. 697–735.
- [11] B. ENGQUIST AND L. YING, *Sweeping preconditioner for the Helmholtz equation: moving perfectly matched layers*, Multiscale Modeling & Simulation, 9 (2011), pp. 686–710.
- [12] S. ESTERHAZY AND J. M. MELENK, *On stability of discretizations of the Helmholtz equation*, in Numerical analysis of multiscale problems, Springer, 2012, pp. 285–324.
- [13] S. FU, E. CHUNG, AND G. LI, *Edge multiscale methods for elliptic problems with heterogeneous coefficients*, Journal of Computational Physics, 396 (2019), pp. 228–242.
- [14] S. FU AND K. GAO, *A fast solver for the Helmholtz equation based on the generalized multiscale finite-element method*, Geophysical Journal International, 211 (2017), pp. 797–813.
- [15] S. FU, G. LI, R. CRASTER, AND S. GUENNEAU, *Wavelet-based edge multiscale finite element method for Helmholtz problems in perforated domains*, arXiv preprint arXiv:1906.08453, (2019).
- [16] D. GALLISTL AND D. PETERSEIM, *Stable multiscale Petrov-Galerkin finite element method for high frequency acoustic scattering*, Computer Methods in Applied Mechanics and Engineering, 295 (2015), pp. 1–17.
- [17] I. GRAHAM AND S. SAUTER, *Stability and finite element error analysis for the Helmholtz equation with variable coefficients*, Mathematics of Computation, 89 (2020), pp. 105–138.
- [18] I. G. GRAHAM, O. R. PEMBERY, AND E. A. SPENCE, *The Helmholtz equation in heterogeneous media: a priori bounds, well-posedness, and resonances*, Journal of Differential Equations, 266 (2019), pp. 2869–2923.
- [19] J. A. GRIEPENTROG AND L. RECKE, *Linear elliptic boundary value problems with non-smooth data: normal solvability on Sobolev–Campanato spaces*, Mathematische Nachrichten, 225

- (2001), pp. 39–74.
- [20] M. HAUCK AND D. PETERSEIM, *Multi-resolution localized orthogonal decomposition for Helmholtz problems*, arXiv preprint arXiv:2104.11190, (2021).
 - [21] P. HENNING AND D. PETERSEIM, *Oversampling for the multiscale finite element method*, Multiscale Modeling & Simulation, 11 (2013), pp. 1149–1175.
 - [22] T. Y. HOU AND P. LIU, *Optimal local multi-scale basis functions for linear elliptic equations with rough coefficient*, Discrete and Continuous Dynamical Systems, 36 (2016), pp. 4451–4476.
 - [23] T. Y. HOU AND X.-H. WU, *A multiscale finite element method for elliptic problems in composite materials and porous media*, Journal of Computational Physics, 134 (1997), pp. 169 – 189.
 - [24] D. LAFONTAINE, E. A. SPENCE, AND J. WUNSCH, *For most frequencies, strong trapping has a weak effect in frequency-domain scattering*, arXiv preprint arXiv:1903.12172, (2019).
 - [25] A. MÅLQVIST AND D. PETERSEIM, *Localization of elliptic multiscale problems*, Mathematics of Computation, 83 (2014), pp. 2583–2603.
 - [26] J. MELENK AND S. SAUTER, *Convergence analysis for finite element discretizations of the Helmholtz equation with Dirichlet-to-Neumann boundary conditions*, Mathematics of Computation, 79 (2010), pp. 1871–1914.
 - [27] J. M. MELENK AND S. SAUTER, *Wavenumber explicit convergence analysis for Galerkin discretizations of the Helmholtz equation*, SIAM Journal on Numerical Analysis, 49 (2011), pp. 1210–1243.
 - [28] A. MOIOLA AND E. A. SPENCE, *Acoustic transmission problems: wavenumber-explicit bounds and resonance-free regions*, Mathematical Models and Methods in Applied Sciences, 29 (2019), pp. 317–354.
 - [29] A. A. OBERAI AND P. M. PINSKY, *A multiscale finite element method for the Helmholtz equation*, Computer Methods in Applied Mechanics and Engineering, 154 (1998), pp. 281–297.
 - [30] M. OHLBERGER AND B. VERFÜRTH, *A new heterogeneous multiscale method for the Helmholtz equation with high contrast*, Multiscale Modeling & Simulation, 16 (2018), pp. 385–411.
 - [31] H. OWHADI, *Multigrid with rough coefficients and multiresolution operator decomposition from hierarchical information games*, SIAM Review, 59 (2017), pp. 99–149.
 - [32] H. OWHADI AND C. SCOVEL, *Operator-Adapted Wavelets, Fast Solvers, and Numerical Homogenization: From a Game Theoretic Approach to Numerical Approximation and Algorithm Design*, vol. 35, Cambridge University Press, 2019.
 - [33] H. OWHADI, L. ZHANG, AND L. BERLYAND, *Polyharmonic homogenization, rough polyharmonic splines and sparse super-localization*, ESAIM: Mathematical Modelling and Numerical Analysis, 48 (2014), pp. 517–552.
 - [34] D. PETERSEIM, *Eliminating the pollution effect in Helmholtz problems by local subscale correction*, Mathematics of Computation, 86 (2017), pp. 1005–1036.
 - [35] D. PETERSEIM AND B. VERFÜRTH, *Computational high frequency scattering from high-contrast heterogeneous media*, Mathematics of Computation, 89 (2020), pp. 2649–2674.
 - [36] J. POULSON, B. ENGQUIST, S. LI, AND L. YING, *A parallel sweeping preconditioner for heterogeneous 3D Helmholtz equations*, SIAM Journal on Scientific Computing, 35 (2013), pp. C194–C212.
 - [37] S. SAUTER AND C. TORRES, *Stability estimate for the Helmholtz equation with rapidly jumping coefficients*, Zeitschrift für angewandte Mathematik und Physik, 69 (2018), p. 139.
 - [38] L. TARTAR, *An introduction to Sobolev spaces and interpolation spaces*, vol. 3, Springer Science & Business Media, 2007.